Identification of Greb1l as a genetic determinant of crisscross heart in mice showing torsion of the heart tube by shortage of progenitor cells

Ségolène Bernheim, Adrien Borgel, Jean-François Le Garrec, Emeline Perthame, Audrey Desgrange, Cindy Michel, Laurent Guillemot, Sébastien Sart, Charles Baroud, Wojciech Krezel, et al.

Identification of *Greb1l* as a genetic determinant of crisscross heart in mice showing torsion of the heart tube by shortage of progenitor cells

Ségolène Bernheim,[1] Adrien Borgel,[1] Jean-François Le Garrec,[1] Emeline Perthame,[1,2] Audrey Desgrange,[1] Cindy Michel,[1] Laurent Guillemot,[1] Sébastien Sart,[3] Charles N. Baroud,[3,4] Wojciech Krezel,[5] Francesca Raimondi,[6,7] Damien Bonnet,[7] Stéphane Zaffran,[8] Lucile Houyel,[7] and Sigolène M. Meilhac[1,9,*]

[1]Université Paris Cité, *Imagine*—Institut Pasteur, Unit of Heart Morphogenesis, INSERM UMR1163, 75015 Paris, France
[2]Institut Pasteur, Université Paris Cité, Bioinformatics and Biostatistics Hub, 75015 Paris, France
[3]Institut Pasteur, Université Paris Cité, Physical Microfluidics and Bio-Engineering, Department of Genomes and Genetics, 75015 Paris, France
[4]Laboratoire d'Hydrodynamique, CNRS, École polytechnique, Institut Polytechnique de Paris, 91120 Palaiseau, France
[5]Institut de Génétique et de Biologie Moléculaire et Cellulaire, Institut de la Santé et de la Recherche Médicale (U1258), Centre National de la Recherche Scientifique (UMR7104), Université de Strasbourg, Fédération de Médecine Translationnelle de Strasbourg, 67404 Illkirch, France
[6]Pediatric Radiology Unit, Hôpital universitaire Necker-Enfants Malades, APHP, Université Paris Cité, 149 Rue de Sèvres, 75015 Paris, France
[7]M3C-Necker, Hôpital universitaire Necker-Enfants Malades, APHP, Université Paris Cité, 149 Rue de Sèvres, 75015 Paris, France
[8]Aix Marseille Université, INSERM, MMG, U1251, Marseille, France
[9]Lead contact
*Correspondence: sigolene.meilhac@institutimagine.org
https://doi.org/10.1016/j.devcel.2023.09.006

SUMMARY

Despite their burden, most congenital defects remain poorly understood, due to lack of knowledge of embryological mechanisms. Here, we identify *Greb1l* mutants as a mouse model of crisscross heart. Based on 3D quantifications of shape changes, we demonstrate that torsion of the atrioventricular canal occurs together with supero-inferior ventricles at E10.5, after heart looping. Mutants phenocopy partial deficiency in retinoic acid signaling, which reflect overlapping pathways in cardiac precursors. Spatiotemporal gene mapping and cross-correlated transcriptomic analyses further reveal the role of *Greb1l* in maintaining a pool of dorsal pericardial wall precursor cells during heart tube elongation, likely by controlling ribosome biogenesis and cell differentiation. Consequently, we observe growth arrest and malposition of the outflow tract, which are predictive of abnormal tube remodeling in mutants. Our work on a rare cardiac malformation opens novel perspectives on the origin of a broader spectrum of congenital defects associated with *GREB1L* in humans.

INTRODUCTION

Tubes are basic structural components of several organs, transporting metabolites. Yet, they acquire specific shapes for specific functions. The heart initially forms as a straight tube in the early embryo, sustaining a single blood flow. Cardiac regions are added sequentially along the tube axis, so that emergence of the double blood circulation during mammalian development is associated with remodeling of the heart tube. An important step is the looping of the heart tube, which positions cardiac chambers, before the partitioning of the left and right cardiac flows.[1]

Failure to establish the double blood circulation during development is a life-threatening condition, by impairment of the overall blood oxygenation level. Collectively congenital heart defects are common, affecting 1% of births, but individually may correspond to rare disorders, requiring expert diagnosis. Currently, most structural congenital heart defects have an unknown genetic origin.[2] Crisscross heart is an example of a very rare congenital heart defect (frequency of 1/125,000 births), with unknown genetic and embryological origins.[3] Crisscross heart is defined by abnormal atrioventricular connections, such that the mitral and tricuspid valves are not localized on the same plane, resulting in crossing of the left and right blood flows.[4] Crisscross heart is almost always associated with other cardiac defects, including malalignments (supero-inferior ventricles, malposition of the great arteries such as double outlet right ventricle), and right-sided obstruction (pulmonary stenosis, right ventricle hypoplasia).[5–7] Based on anatomical observations, it has been hypothesized (1) that crisscross heart results from a twist of ventricles following septation[4,5,8] or (2) that ventricle malposition reflects defective heart looping.[9,10] Yet, these hypotheses have never been tested experimentally, by lack of an animal model.

Remodeling of the heart tube has been investigated in animal models. Shape changes are concomitant with the elongation of

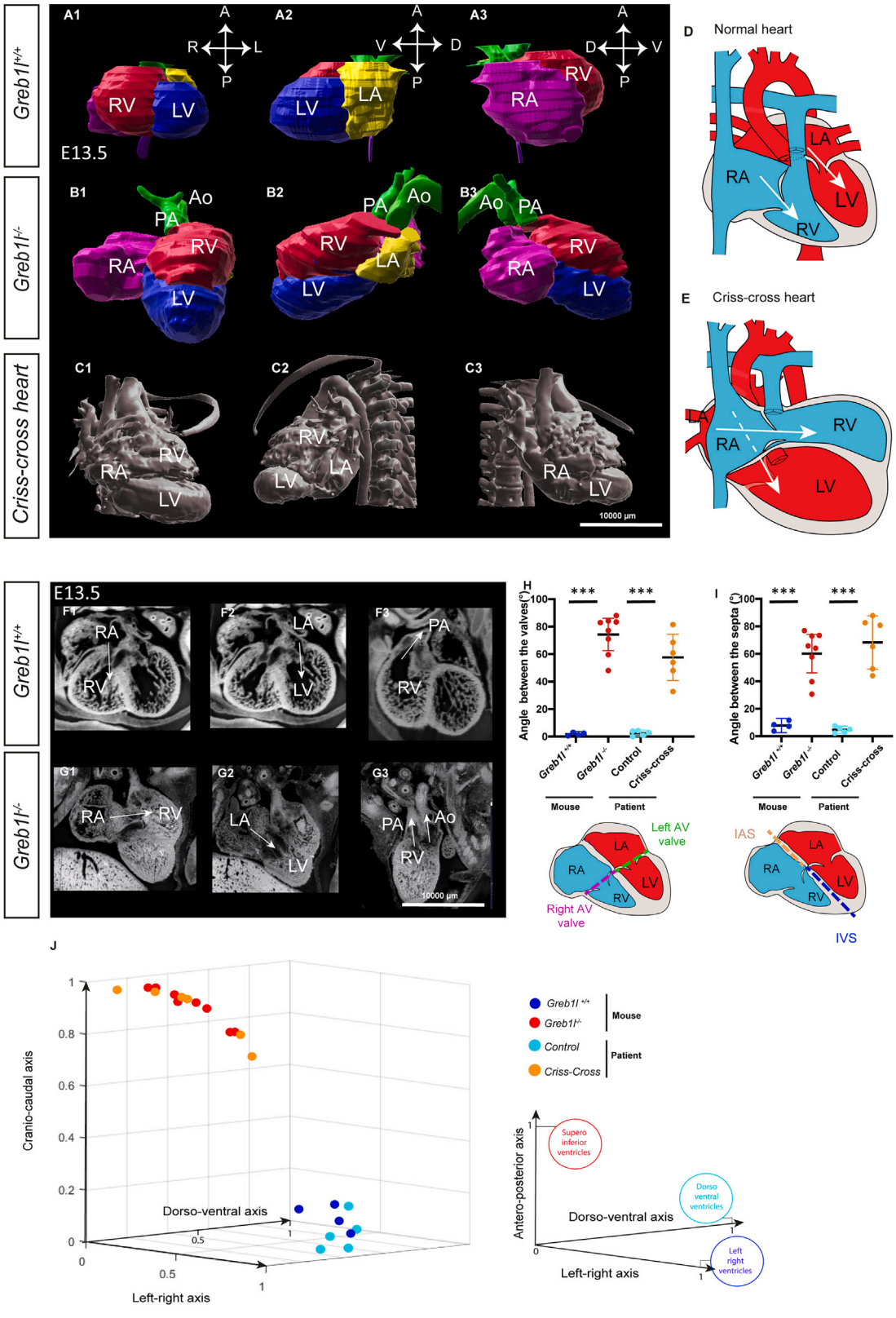
Greb1l+/+
Greb1l-/-
Criss-cross heart
A1
A2
A3
E13.5
RV
LV
LA
RA
B1
B2
B3
Ao
PA
C1
C2
C3
10000 µm
D
Normal heart
E
Criss-cross heart
E13.5
F1
F2
F3
G1
G2
G3
H
Angle between the valves(°)
***
Greb1l +/+
Greb1l -/-
Control
Criss-cross
Mouse
Patient
Left AV valve
Right AV valve
I
Angle between the septa (°)
IAS
IVS
J
Cranio-caudal axis
Dorso-ventral axis
Left-right axis
Mouse
Patient
Antero-posterior axis
Supero inferior ventricles
Dorso ventral ventricles
Left right ventricles

the tube, by ingression of heart precursors at both poles. In the mouse, elongation of the tube occurs, while the distance between the poles remains fixed. This is the basis of a buckling mechanism, central to the process of heart looping at E8.5, thus highlighting the importance of mechanical constraints.[11] Cell ingression continues after heart looping and is important for the elongation of the outflow tract.[12,13] However, how this later ingression affects the shape of the whole heart tube has been overlooked. Cell ingression is coupled with cell differentiation: the heart tube is composed of a myocardium layer, whereas cells in continuity with the tube, in the dorsal pericardial wall, are a reservoir of undifferentiated cardiac precursors, referred to as the second heart field.[14] Markers associated with cardiomyocyte differentiation are now extensively documented by recent profiling of single embryonic cardiac cells.[15,16] Based on clonal analyses and genetic tracing, the progressive ingression of cells fated to specific cardiac regions has been reconstructed[17]: the posterior second heart field, for example, contributes to both poles of the heart, including the atria and the inferior outflow tract, the source of the pulmonary trunk.[18,19] Cell ingression and heart tube elongation are regulated by multiple factors, including cardiomyocyte differentiation factors, cell proliferation factors, as well as regulators of epithelial architecture.[12,20–22] Cell ingression is also modulated by patterning cues, which provide dynamic positional information at specific stages. For example, transient Nodal signaling in the left heart field biases cell behavior to control the asymmetric remodeling of the heart tube during heart looping.[23] Retinoic acid (RA), a metabolite of vitamin A, patterns the heart field in the antero-posterior axis and controls its size, with a dose-sensitive effect.[24–26]

Greb1l has been identified in embryonic stem (ES) cells as a target of RA, activated upon RA stimulation.[27] In humans, *GREB1L* is associated with a broad spectrum of congenital defects, including renal agenesis, hearing impairment, thymic, genital, and skeletal anomalies[28]: 49 *de novo* or inherited deleterious dominant alterations of *GREB1L* have been identified, underlining its importance as a disease-causing gene. In the mouse, knockout of *Greb1l* is homozygous lethal at fetal stages, reproducing several human defects, with additional defects in the heart and brain.[29] GREB1L has no characterized function, but its paralogue GREB1 has been shown to have glycosyl-transferase activity.[30] Thus, pathological mechanisms upon *Greb1l* inactivation have remained enigmatic, by lack of knowledge of its function, as well as of the cells in which it is active.

Here, we identify *Greb1l* mutants as a mouse model of crisscross heart with supero-inferior ventricles. Based on quantitative analyses of gene expression and shape changes, taking into account the spatiotemporal dynamics, we address the embryological origin of crisscross heart. Our results demonstrate that *Greb1l* is not required for heart looping, but for outflow tract growth thereafter, thus maintaining the overall heart tube shape. With tailored transcriptomic analyses, we further show that *Greb1l* is required to maintain a pool of cardiac precursors, regulating not only cardiomyocyte differentiation but also ribosome biogenesis. We find that *Greb1l* mutants phenocopy partial deficiency in RA signaling, without any obvious interaction with it. Overall, our work identifies *Greb1l* as a genetic determinant of crisscross heart in mice and unravel pathological mechanisms, potentially relevant to other congenital defects.

RESULTS

Greb1l mouse mutants model human crisscross heart

We analyzed in more detail *Greb1l* mouse mutants, which were previously reported to have heart defects with chamber malalignment.[29] *Greb1l*$^{-/-}$ fetuses were collected at E13.5, before lethality and at the end of ventricular septation.[31] In 3D images of the heart, we observed an abnormal supero-inferior (i.e., cranio-caudal) position of the ventricles, compared with the left-right position in controls (Figures 1A and 1B; Video S1). The atria were normally positioned and atrioventricular connections crossed each other (Figures 1F and 1G). The aorta and pulmonary trunk were correctly septated but parallel and both connected to the right ventricle (Figures 1A, 1B, 1F, 1G, S1N, and S1O; Video S2), indicative of double outlet right ventricle with full penetrance. Crossing of atrioventricular connections is a very rare feature of congenital heart defects, diagnostic of crisscross heart (Figures 1D and 1E), not reported in heterotaxy,[32] which is classically associated with cardiac chamber malalignment. Since crisscross heart has never been reported in mice, we quantified the heart structure comparatively in *Greb1l* mouse mutants and patients with the same phenotype, i.e., crisscross heart with supero-inferior ventricles (Figure 1C). The planes of the left and right atrioventricular valves were found at a 74° ± 10° angle in *Greb1l* mouse mutants, which is non-significantly different from the 57° ± 17° angle in diseased patients, and significantly different from the null value in both mouse and patient controls (Figure 1H). Consistently, the planes of the interatrial and interventricular septa were found at an average 60° angle in *Greb1l* mouse mutants and 68° in diseased patients, whereas they are parallel in control hearts (Figure 1I). Finally, the 3D orientation of the right ventricle-left ventricle axis was

Figure 1. Quantification of structural heart defects in *Greb1l* mouse mutants at E13.5 by comparison with human crisscross heart

(A and B) 3D segmented heart from HREM in controls (A) and *Greb1l*$^{-/-}$ mutants (B) in ventral (A1–B1), left- (A2–B2), and right-side (A3–B3) views.

(C) 3D segmented heart from a patient CT-scan with crisscross heart and supero-inferior ventricles.

(D and E) Schema of the structure of crisscross heart (E) compared with normal (D).

(F and G) Coronal sections of control (F) and *Greb1l* mutant (G) hearts, showing atrioventricular (arrows, F1–G2) and ventriculo-arterial (arrows, F3–G3) connections.

(H) Quantification of the angle between the left and right atrioventricular (AV) valves in mouse and patient hearts.

(I) Quantification of the angle between the interatrial (IAS) and interventricular (IVS) septa in mouse and patient hearts. ***p value < 0.001 (one-way ANOVA, n = 4 *Greb1l*$^{+/+}$, 8 *Greb1l*$^{-/-}$, 5 control patients, 6 diseased patients).

(J) 3D coordinates of the RV/LV axis in mice and patients displaying crisscross hearts with supero-inferior ventricles compared with controls. Means and standard deviations are shown. A, anterior; Ao, aorta; D, dorsal; L, left; LA, left atrium; LV, left ventricle; n, number of observations; P, posterior; PA, pulmonary artery; R, right; RA, right atrium; RV, right ventricle; V, ventral.

See also Videos S1 and S2.

quantified in the endogenous context of the thoracic cavity. In both *Greb1l* mouse mutants and diseased patients, the ventricles clearly aligned with the cranio-caudal axis, as distinct from control hearts (Figure 1J). We have thus identified a mouse model of the crisscross heart disease, with a full penetrance, opening the possibility to investigate the etiology of this poorly understood congenital heart defect.

Greb1l is expressed in cardiac precursors

Despite the involvement of *GREB1L* in several congenital defects,[28] its expression profile during development has been poorly characterized. We imaged this in 3D at sequential stages of heart development. In addition to expression in the neural tube, endoderm, and posterior paraxial mesoderm, we detected *Greb1l* in the lateral plate mesoderm, including cardiac cells, from the late headfold stage (Figures 2A and 2B; Video S3 and data not shown). Cardiac expression is transient, maximal at E8.5c,d, and by E9.5, it was no longer discernible (Figures 2B–2D). Within the forming heart tube, *Greb1l* was expressed in the myocardium and endocardium (Figures 2B4–2C4). However, expression was found 7-fold higher in the heart field compared with the heart tube (Figure 2E). These observations are supported by published single-cell transcriptomics of cardiac cells,[15] where *Greb1l* levels are higher in myocardial precursor clusters Me5 (juxta-cardiac field) and Me7 (second heart field) and higher at crescent stages. Compared with *Greb1l*-negative cells, *Greb1l*-positive cells in Me3–Me7 clusters show increased proliferation capacity, with a lower proportion of cells in G1 (Figure 2F). We identified the genes that significantly correlated with variations in *Greb1l* expression levels in the single-cell dataset. The top genes most significantly negatively correlated with *Greb1l* correspond to the cardiomyocyte differentiation genes *Actc1*, *Myl4/7*, *Tmp1*, *Tnnt2*, and *Tnni1* (Figure 2G). Overall, we conclude that *Greb1l* is expressed in early cardiac precursors, before and at the time of heart tube formation.

Greb1l is not required for heart looping

We noticed similarities between *Greb1l* and *Nodal*[23]: both genes are expressed in cardiomyocyte precursors before the formation of the heart tube, and both are required for ventricle position. We thus hypothesized that *Greb1l* could be required, similar to *Nodal*, for heart looping, the process during which the right ventricle, initially formed cranially, acquires its position on the right side of the left ventricle. We quantified in *Greb1l* mutants the 3D shape of the heart tube at E9.5, when heart looping is complete in controls. We observed a right-sided position of the right ventricle in E9.5 mutants (Figures 3A and 3B; Video S4), not significantly different from controls (Figure 3G), as well as normal patterning of the heart tube, as seen with the cardiac chamber marker *Nppa* (Figures 3C and 3D) and left markers *Wnt11* and *Bmp2* (Figures 3E and 3F). We have shown previously that heart looping results from a buckling mechanism[11]: the associated parameters of heart tube length and distance between the poles did not significantly change in *Greb1l* mutants at E9.5 (Figures 3H–3J). In an independent mutant line that targets a different exon, $Greb1l^{ex17/ex17}$, we again did not detect anomalies of heart looping (Figures S1A and S1D). Taken together, our 3D analyses show that *Greb1l* is not required for heart looping.

Greb1l is required to maintain ventricle position after heart looping

Given the correct position of ventricles in the embryonic E9.5 heart tube of *Greb1l* mutants, we analyzed the kinetics of heart shape changes until the crisscross heart phenotype seen at E13.5. We observed a dramatic change at E10.5, with no further deterioration at subsequent stages (Figures S1F–S1O). This kinetics was similarly observed in the two mutant lines, with 100% penetrance (Figures S1A–S1E). At E10.5, the ventricles of *Greb1l* mutants have become supero-inferior (Figures 3K, 3L, and 3Q; Video S5), whereas patterning of the heart, with the cardiac chamber marker *Nppa* (Figures 3M and 3N) and left marker *Pitx2* (Figures 3O and 3P) was unaffected. Thus, *Greb1l* is required to maintain ventricle position after heart looping, without affecting heart tube patterning.

Growth arrest of the outflow tract and reduction of pole distance are predictive of ventricle position

Changes in ventricle position in *Greb1l* mutants was accompanied by additional defects at E10.5. The distance between the heart tube poles was significantly reduced in *Greb1l* mutants, in both the left-right and cranio-caudal axes (Figures 4A and 4B). The heart tube length was significantly decreased, as a result of a significant shortening of the outflow tract (Figures 4C and 4D), whereas the rest of the tube had a constant length (888 ± 175 μm in 6 controls compared with 841 ± 95 μm in 8 mutants, $p = 0.5$, t test). Cushions of the atrioventricular canal, which are parallel and supero-inferior in control hearts, had a spiraling pattern in *Greb1l* mutants (Figures 4E and 4F). Spiraling of cushions is normally a feature of the outflow tract,[33] reflecting its rightward rotation.[34] We detect here an exceptional case of spiraling of atrioventricular cushions, which thus indicates abnormal leftward rotation of the atrioventricular canal in *Greb1l* mutants. Given that cushions are precursors of the valves, rotation of atrioventricular cushions is consistent with the later phenotype of crisscross heart. Finally, outflow cushions, had spiraling defects in *Greb1l* mutants (absence of spiraling or abnormal direction of rotation, $n = 5$) (Figures S1P–S1U). Outflow tract defects (shortening and abnormal spiraling) are consistent with the later phenotype of double outlet right ventricle.

To understand the mechanism of abnormal ventricle position, we investigated which geometrical parameters were more closely associated with ventricle position, using a generalized linear model. The standardized Akaike information criterion (AIC), which measures the quality of alternative predictive models, was best when we considered both the outflow tract length and the left-right distance between the heart tube poles as predictive variables (Figure 4G) and indeed was very close to the AIC of a reference model using the genotype as a variable. We then analyzed the kinetics of these parameters in relation to ventricle position. Between E9.5 and E10.5, whereas the outflow tract grows 2-fold in control hearts (325 ± 112 μm in $n = 8$ E9.5 compared with 644 ± 116 μm in $n = 6$ E10.5, $p < 0.0001$, t test), growth was completely arrested in *Greb1l* mutants (309 ± 112 μm in 7 E9.5 compared with 380 ± 62 μm in 9 E10.5, $p = 0.13$, t test) and the length of the OFT at E10.5 was a strong linear predictor ($R^2 = 0.75$) of ventricle position (Figures 4H–4J). During the same time window, the left-right distance between the heart tube poles, which tends to be stable in

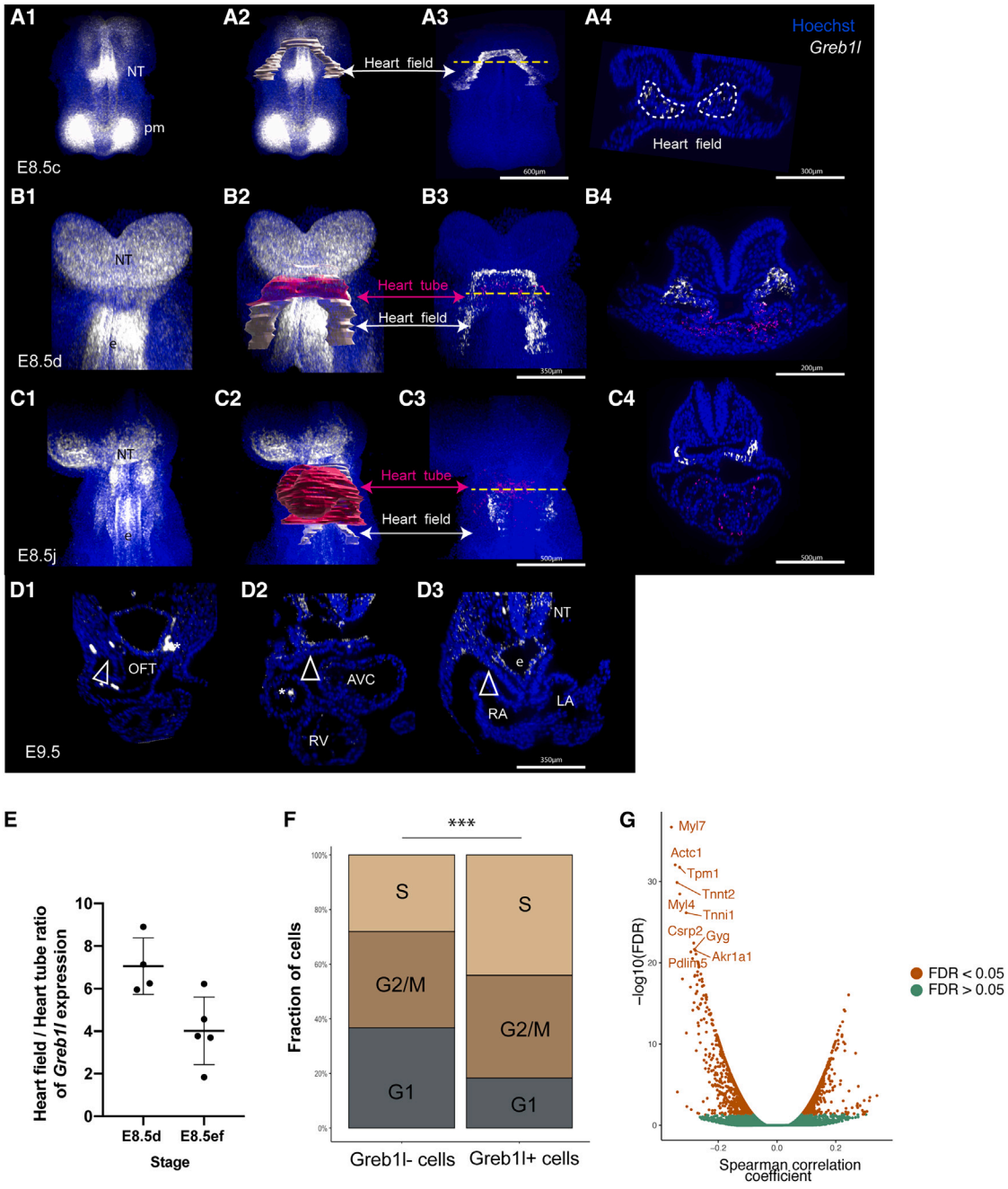

Figure 2. Expression pattern of *Greb1l* at E8.5

(A–C) Expression of *Greb1l* (white) detected by whole-mount RNAscope ISH in control embryos at E8.5c (A), E8.5d (B), and E8.5j (C), shown in a ventral view (A1–C3) and in transversal sections (A4–C4) at the levels indicated in (A3)–(C3). Segmentation of cardiac tissues is indicated in (A2)–(C2), including the heart field (white) and heart tube (red). Expression of *Greb1l* within the segmented domains is shown in (A3)–(C3), with the same color code.

(D) Expression of *Greb1l* at E9.5 in serial transverse sections, from anterior to posterior (n = 3). Arrows point to the negative heart field. Asterisks, unspecific aggregates.

(E) Corresponding quantification of the relative expression of *Greb1l* in the heart field and heart tube at the indicated stages (n = 4 E8.5d, 5 E8.5e,f). Means and standard deviations are shown.

(F) Fraction of wild-type embryonic cardiac cells[15] assigned transcriptionally to the different cell cycle phases (n = 1,383 *Greb1l*+ and 485 *Greb1l*− cells). ***p < 0.001 (chi-squared test).

(G) Volcano plot for co-expression analysis with *Greb1l* expression levels. Spearman correlation between genes of the dataset,[15] and *Greb1l* expression levels in single embryonic cardiac cells is represented against its significance (n = 1,868 cells, Benjamini-Hochberg-corrected p value < 0.05 in brown and >0.05 in green).

AVC, atrioventricular canal; e, endoderm; FDR, false discovery rate; LA, left atrium; LV, left ventricle; NT, neural tube; OFT, outflow tract; pm, paraxial mesoderm; RA, right atrium; RV, right ventricle.

See also Video S3.

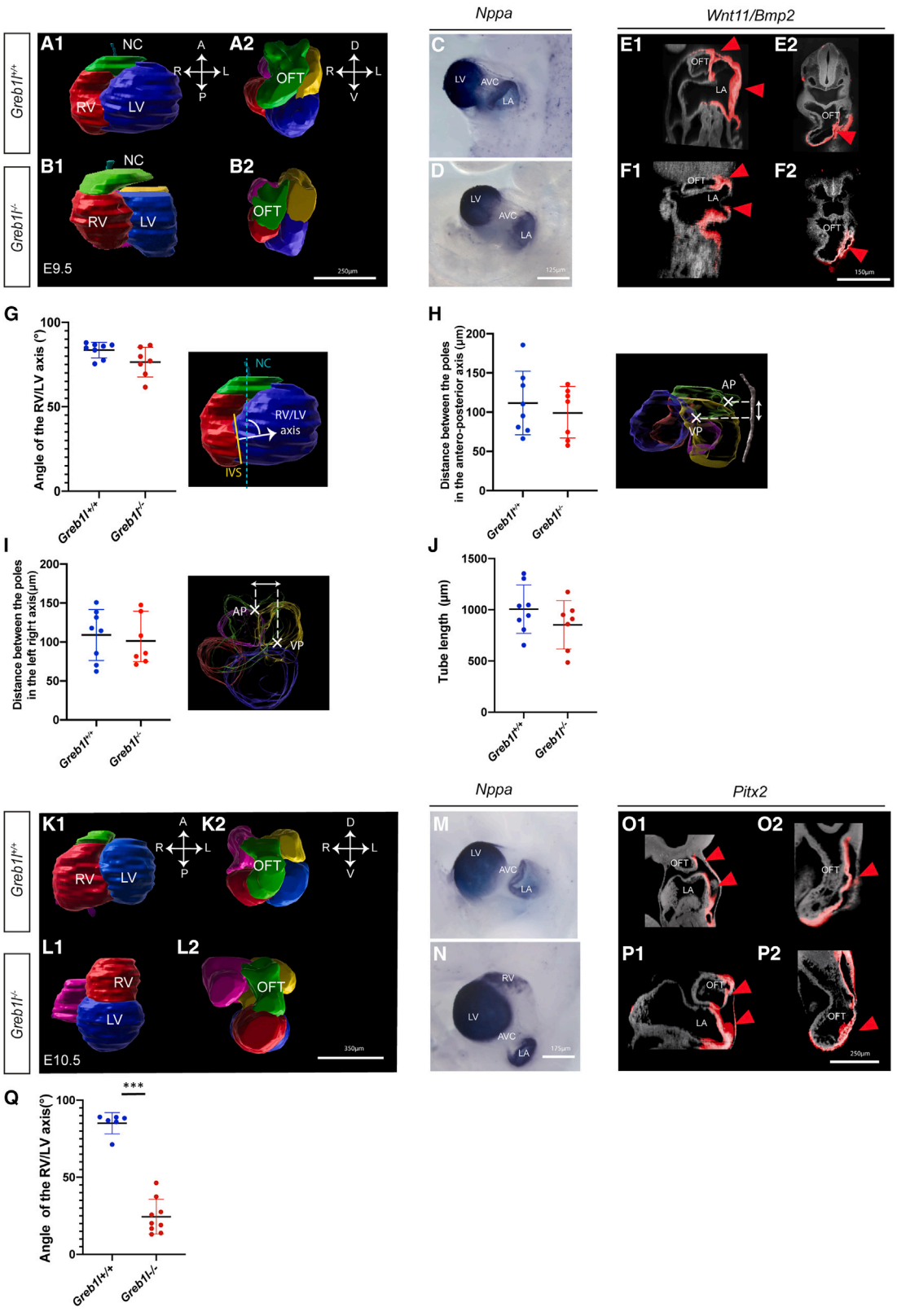
Nppa
Wnt11/Bmp2
Greb1l+/+
Greb1l-/-
A1
NC
RV
LV
A
R
L
P
A2
OFT
D
V
B1
B2
E9.5
250μm
C
LV
AVC
LA
D
125μm
E1
E2
OFT
LA
F1
F2
150μm
G
Angle of the RV/LV axis (°)
100
50
0
Greb1l+/+
Greb1l-/-
NC
RV/LV axis
IVS
H
Distance between the poles in the antero-posterior axis (μm)
200
150
100
50
0
AP
VP
I
Distance between the poles in the left right axis(μm)
J
Tube length (μm)
1500
1000
500
Nppa
Pitx2
K1
K2
L1
L2
E10.5
350μm
M
N
RV
O1
O2
P1
P2
250μm
Q
***
Angle of the RV/LV axis(°)

control hearts, was significantly reduced in *Greb1l* mutants, this distance being also a linear predictor of the ventricle position, although to a lesser extent (R^2 = 0.37) (Figures 4K–4M).

Our quantitative anatomical analyses, together with the observations that *Greb1l* is mainly expressed outside the heart tube and that the heart tube is patterned normally in the mutant, suggest a mechanical process of ventricle malpositioning. We propose a model in which differential growth in the outflow tract relative to the rest of the heart tube, as well as reduction of pole distance, exert a constraint, which pulls the tube toward the arterial pole. Since the atrioventricular canal is the section of the heart tube with the least resistance to torsion (Figure 4N), pulling would result in twisting at the atrioventricular canal (Figure 4O).

Greb1l mutants phenocopy partial RA deficiency

Greb1l has been shown previously to be a direct target of RA receptors[27] and RA signaling is required for outflow tract growth.[26,35,36] These led us to investigate the relationship between *Greb1l* and RA signaling. We first analyzed the expression pattern of *Greb1l* relative to that of *Aldh1a2*, encoding the main RA synthesizing enzyme, and of the transgenic reporter *RARE-lacZ*. In the heart field, *Aldh1a2* was expressed in the most posterior third, overlapping with *Greb1l*, which covers the whole heart field (Figure S2B). *RARE-lacZ* extended more anteriorly over two-thirds, also overlapping with *Greb1l* (Figure S2A). This indicates that *Greb1l* is expressed within the RA responsive domain but also extends more broadly. Genetic tracing with either *RARE-lacZ* or *RARE-CreERT2;R26*$^{mTmG/+}$ shows that RA responsive cells are fated to the outflow tract myocardium at E8.5j–E9.5, in addition to that of the atria (Figures S3A–3D).

We then investigated whether RA signaling is affected in *Greb1l* mutants, using canonical transcriptional readouts. Abnormal patterning of rhombomeres in *Greb1l* mutants (Figures S3E–S3H), in which rhombomere 4 is present but posteriorized, is a characteristic signature of partial RA deficiency seen in *Hnf1b* and *Rdh10* mutants,[37,38] in contrast to the loss of rhombomere 4 upon complete RA deficiency in *Aldh1a2* mutants.[39] Within the cardiac region, the expression profile of two RA responsive genes, *Tbx5* and *Fgf8*,[40–43] were expanded posteriorly in *Greb1l* mutants compared with control embryos (Figures S2D–S2G). This abnormal molecular patterning phenocopies RA deficiency in *Aldh1a2* and *Rdh10* mutant embryos.[40,41,43] At a morphological level, complete RA deficiency in *Aldh1a2* mutants is more severe than *Greb1l* mutants: earlier lethality (E10.5), early defects in heart tube formation.[41,42] Thus, we focused on a model of partial RA deficiency, in which another RA synthesizing enzyme, Rdh10, is targeted. *Rdh10* mutants were reported to survive until E12.5 with a milder phenotype of "misaligned putative ventricles."[37] We analyzed this into more detail. At E10.5, 5/14 (35%) Rdh10$^{-/-}$ embryos had abnormal supero-inferior ventricles and spiral atrioventricular cushions indicative of crisscross heart, with variable severity (Figures S2H–S2J). This was associated with a reduction in the left-right pole distance, but not with a shorter outflow tract (Figures S2K–S2M). Thus, our analyses show that partial RA deficiency in *Rdh10* mutants also leads to crisscross heart with supero-inferior ventricles and reduction in the left-right pole distance. Molecular patterning and morphological observations both support striking similarities between *Greb1l* inactivation and partial RA deficiency.

To understand whether the two pathways interact, we monitored RA response in *Greb1l* mutants, based on the expression of the transgenic reporter *RARE-lacZ*. This was largely unaffected in *Greb1l* mutants, with a similar anterior boundary of expression (Figures S2N and S2O). The less posterior transgene boundary is in keeping with the phenotypic posterior truncation. The maintenance of *RARE-lacZ* in *Greb1l* mutants thus differs from its absence in *Aldh1a2* and *Rdh10* mutants.[44,45] We next performed a transcriptomic profiling of the cardiac region in *Greb1l* mutant compared with control embryos at E8.5e (Figure S2P), at the end of the time window of *Greb1l* expression in controls. After quality check (Figures S4A–S4C), we identified significantly differentially expressed genes in both *Greb1l* mutant lines. In agreement with the *RARE-lacZ* profile, canonical RA targets with functional retinoic-acid-responsive elements (RARE),[46] including *Rarb*, *Fgf8*, *Dhrs3*, *Hoxa1*, and *Fst*, had normal expression levels in *Greb1l* mutants, except *Crabp2*, which was significantly downregulated (Figure S2Q). In addition, expression of *Aldh1a2* and *Rdh10*, which encode the main RA synthesizing enzymes in cardiac cells, were unchanged (Figure S2R). However, other components of the RA pathway were significantly upregulated, including *Por*, *Rai1*, and *Rbp1* (Figure S2S), which is compatible with compensatory mechanisms, as shown previously,[47] of a phenotype equivalent to partial RA deficiency. This suggests overall that GREB1L does not fundamentally affect RA signaling. We finally investigated whether *Greb1l* responds to RA signaling in the mouse embryo, given that *Greb1l* had been reported to be induced in all-trans retinoic acid (ATRA)

Figure 3. Geometry and patterning of the heart tube in *Greb1l* mutant embryos at E9.5–E10.5

(A and B) 3D segmented heart at E9.5 in controls (A) and *Greb1l*$^{-/-}$ mutants (B), shown in frontal (A1–B1) and cranial (A2–B2) views. The notochord (NC) is used as the midline reference axis.

(C and D) *In situ* hybridization of *Nppa*, labeling cardiac chambers, in controls (C, n = 4) and *Greb1l*$^{ex17/ex17}$ mutants (D, n = 4) at E9.5, in a left-sided view.

(E and F) HREM coronal (E1–F1) and transverse (E2–F2) sections of controls (E, n = 4) and *Greb1l*$^{-/-}$ mutants (F, n = 4). The left-sided expression of *Wnt11* and *Bmp2* is in red, the histology in gray.

(G–J) Corresponding quantifications of the RV/LV axis (G), antero-posterior (H), and left-right (I) distance between the heart tube poles, and tube length (J) in controls (n = 8) and *Greb1l*$^{-/-}$ mutants (n = 7) at E9.5 (non-significantly different t test).

(K and L) 3D segmented heart at E10.5 in controls (K) and *Greb1l*$^{-/-}$ mutants (L), shown in frontal (K1–L1) and cranial (K2–L2) views.

(M and N) *In situ* hybridization of *Nppa* in controls (M, n = 3) and *Greb1l*$^{-/-}$ mutants (N, n = 5) at E10.5.

(O and P) HREM coronal (O1–P1) and transverse (O2–P2) sections of controls (O1, n = 3) and mutants (P, n = 4). The left-sided expression of *Pitx2* is in red.

(Q) Corresponding quantification of the RV/LV axis in controls (n = 8) and *Greb1l*$^{-/-}$ mutants (n = 9) at E10.5. ***$p < 0.001$ (Mann-Whitney test). Means and standard deviations are shown. A, anterior; AP, arterial pole; AVC, atrioventricular canal; D, dorsal; IVS, interventricular septum; L, left; LA, left atrium; LV, left ventricle; NC, notochord; R, right; RV, right ventricle; OFT, outflow tract; P, posterior; V, ventral; VP, venous pole.

See also Figure S1; Videos S4 and S5.

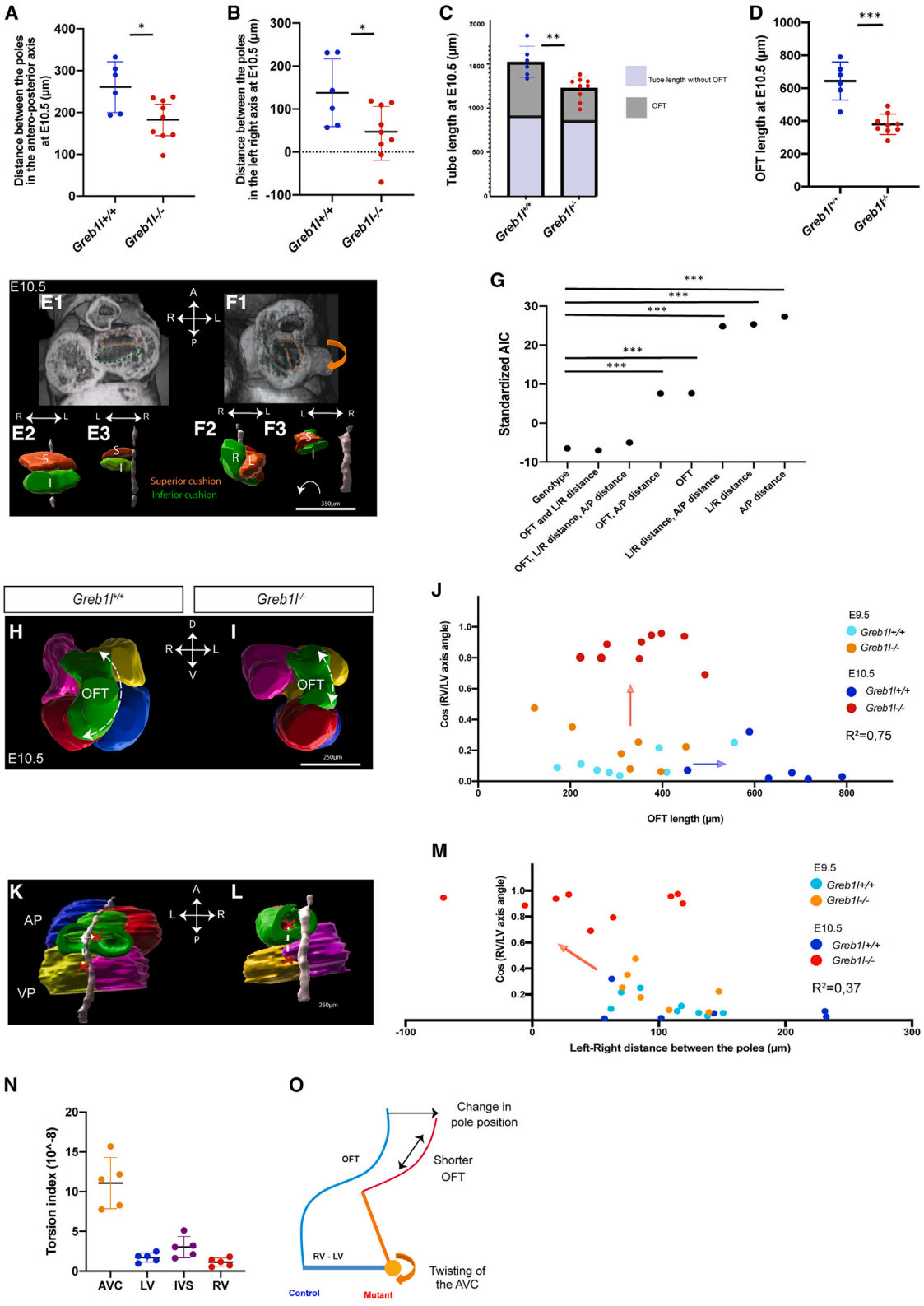
A
Distance between the poles in the antero-posterior axis at E10.5 (µm)
400
300
200
100
0
*
Greb1l+/+
Greb1l-/-
B
Distance between the poles in the left right axis at E10.5 (µm)
300
200
100
0
-100
*
Greb1l+/+
Greb1l-/-
C
Tube length at E10.5 (µm)
2000
1500
1000
500
0
**
Tube length without OFT
OFT
Greb1l+/+
Greb1l-/-
D
OFT length at E10.5 (µm)
1000
800
600
400
200
0
***
Greb1l+/+
Greb1l-/-
E10.5
E1
F1
A
R
L
P
E2
E3
F2
F3
S
I
R
L
Superior cushion
Inferior cushion
350µm
G
Standardized AIC
30
20
10
0
-10
***
***
***
***
***
Genotype
OFT and L/R distance
OFT, L/R distance, A/P distance
OFT, A/P distance
OFT
L/R distance, A/P distance
L/R distance
A/P distance
Greb1l+/+
Greb1l-/-
H
I
D
R
L
V
OFT
OFT
E10.5
250µm
J
Cos (RV/LV axis angle)
1.0
0.8
0.6
0.4
0.2
0.0
0
200
400
600
800
OFT length (µm)
E9.5
Greb1l+/+
Greb1l-/-
E10.5
Greb1l+/+
Greb1l-/-
R²=0,75
K
AP
VP
A
L
R
P
L
250µm
M
Cos (RV/LV axis angle)
1.0
0.8
0.6
0.4
0.2
-100
0
100
200
300
Left-Right distance between the poles (µm)
E9.5
Greb1l+/+
Greb1l-/-
E10.5
Greb1l+/+
Greb1l-/-
R²=0,37
N
Torsion index (10^-8)
20
15
10
5
0
AVC
LV
IVS
RV
O
Change in pole position
OFT
Shorter OFT
RV - LV
Twisting of the AVC
Control
Mutant

treated ES cells.[27] However, in *Aldh1a2* mutants, we did not detect the expected downregulation of *Greb1l* (Figure S3I).

Taken together, our results show that *Greb1l* inactivation phenocopies the specific features of partial RA deficiency, but without any obvious interaction between the two pathways. The phenocopy probably reflects parallel activity in the same population of cardiac precursors.

Greb1l regulates cardiomyocyte differentiation and ribosome biogenesis to maintain the pool of precursor cells

We analyzed the role of *Greb1l* independently of RA signaling, using transcriptomic approaches. We identified 293 genes consistently deregulated in both *Greb1l* mutant lines (Figures 5A and 5B) and selected four genes, *Cacna1h*, *Fabp3*, *Col5a1*, and *Hapln1* to validate differential expression (Figures 5G–5J and S4D–S4H). Then, we intersected differentially expressed genes with the list of genes significantly correlated with variations in *Greb1l* expression levels in single wild-type embryonic cardiac cells (Figures 5B and 5C). Satisfactorily, 88 genes negatively correlated with *Greb1l* in wild-type cells, were significantly upregulated in *Greb1l* mutants, whereas 161 genes positively correlated with *Greb1l* in wild-type cells were significantly downregulated in *Greb1l* mutants (Figure 5C). We have thus identified a set of genes specifically associated with *Greb1l* in embryonic cardiac cells (Table S1). Enrichment analysis of GO pathways singles out two main categories of genes: genes involved in cardiomyocyte differentiation are collectively enriched in *Greb1l* mutants, whereas genes associated with ribosomes are collectively depleted in *Greb1l* mutants (Figures 5D and S4L). We further analyzed targeted gene lists of cardiomyocyte differentiation and ribosomes. This shows that genes specifically involved in terminal cardiomyocyte differentiation (Me3) rather than intermediate cardiomyocyte differentiation (Me4/6) are upregulated in *Greb1l* mutants at E8.5e (Figures 5E and S4I). In addition, genes specifically involved in ribosome biogenesis, rather than ribosome components are downregulated in *Greb1l* mutants at E8.5e (Figures 5F and S4J). *Ncl*, which encodes a major rRNA processing protein,[48] is the most significant gene of the list (correlation FDR = 6.7×10^{-15}, differential expression FDR = 8.4×10^{-22}, Table S1).

To validate this pathway analysis, we used two approaches: *in vivo* labeling and cardiac organoids. Cardiomyocyte differentiation genes such as *Cacna1h* and *Fabp3* were validated as more highly expressed in *Greb1l* mutant hearts at E8.5e (Figures 5G–5J). Similarly, *Ncl* was validated as downregulated in the heart field of *Greb1l* mutants at E8.5j (Figures 5K and 5L). We then modeled cardiac differentiation in mouse organoids. Downregulation of *Greb1l*, using *Greb1l*$^{+/tm1a}$ ES cells (Figures 6A–6D), restrained cardioid formation, compared with wild-type ES cells. This was associated with a depletion of cardiac precursors, as detected by *Tbx1* downregulation. Cardiomyocyte differentiation, based on *Actc1* expression, was initially upregulated at day 4, but severely downregulated in the longer term (days 7–12) (Figure 6E). Indeed, *Greb1l*$^{+/tm1a}$ cardioids failed to beat. When we briefly treated cardioids with an inhibitor of ribosome biogenesis, BMH-21, we transiently impaired the specification of cardiac precursors and cardiomyocyte differentiation (Figures 6F and S5), indicating that the longer term effects of *Greb1l* loss may correspond to secondary effects of decreased ribosome biogenesis.

To assess the cellular response to transcriptional changes observed at E8.5, we analyzed E9.5 embryos. A few cardiomyocytes were abnormally detected in the dorsal pericardial wall of *Greb1l* mutants (Figures 7A1–7B1 and 7C), indicative of premature differentiation. In addition, anomalies in the heart field were detected. The dorsal pericardial wall was found significantly reduced in surface (Figures 7A2–7B3 and 7D), but not in cell number, which is further supported by unchanged cell proliferation and apoptosis (Figure S6). In keeping with a deformation of the heart field, its epithelial architecture was disorganized in *Greb1l* mutants: it was thicker with impaired apicobasal polarity (Figures 7I–7L). Together with decreased *Tbx1* expression in mutant cardioids, this indicates an abnormal specification of the precursor cell reservoir. In addition, the cardiac precursor marker Isl1 was found more inside the heart tube, in the right atrium (Figures 7A4–7B4). Conversely, a more mature cardiomyocyte gene, *Fabp3*, had a reduced expression at the heart

Figure 4. Outflow tract and atrioventricular canal defects in *Greb1l* mutants at E10.5

(A and B) Quantification of the antero-posterior (A) and left-right (B) distance between the heart tube poles in controls (n = 8) and mutants (n = 9) at E10.5. *p value < 0.05 (t test).

(C and D) Quantification of the heart tube length at E10.5 in the same samples, showing the contribution of the outflow tract (OFT, gray in C and D) relative to the rest of the tube (pale blue in C). **p < 0.01 (t test).

(E and F) 3D images by HREM showing coronal sections of atrioventricular cushions in control (E) and *Greb1l* mutants (F) and associated 3D segmentations in ventral (E2–F2) and dorsal (E3–F3) views. Superior (S) and inferior (I) cushions (proximally) are in orange and green respectively, the notochord in gray. The orientation of cushion spiraling is indicated by an arrow.

(G) Evaluation of a generalized linear model for the indicated combination of parameters, based on the standardized Akaike information criterion (AIC), which is lower in better models. ***relative likelihood < 0.001 (n = 15).

(H and I) 3D segmented heart at E10.5 in a cranial view. Arrows outline differential lengths of the outflow tract in controls and mutants.

(J) Correlation between the outflow tract length (x) and the RV/LV axis (y), shown at E9.5 (paler colors) and E10.5 (darker colors) in controls (blue) and mutants (orange and red). Significant changes between stages are indicated by arrows. R^2, Pearson determination coefficient at E10.5 (n = 7 and 6 controls at E9.5 and E10.5, 7, and 9 mutants at E9.5 and E10.5, respectively).

(K and L) 3D segmented heart at E10.5 in a dorsal view. Arrows indicate differential left-right distances between the poles (red crosses) in controls and mutants.

(M) Correlation between the left-right pole distance (x) and the RV/LV axis (y) shown as in (J).

(N) Torsion index calculated for heart tube regions. Mean values and standard deviations are shown for 5 control hearts at E10.5.

(O) Schematic representation of the proposed mechanical mechanism, whereby twisting (orange arrow) of the AVC results from growth arrest in the OFT and reduced pole distance. The control and mutant situations are in blue and orange, respectively. Means and standard deviations are shown. A, anterior; AP, arterial pole; AVC, atrioventricular canal; D, dorsal; IVS, interventricular septum; L, left; LV, left ventricle; R, right; RV, right ventricle; OFT, outflow tract; P, posterior; V, ventral; VP, venous pole.

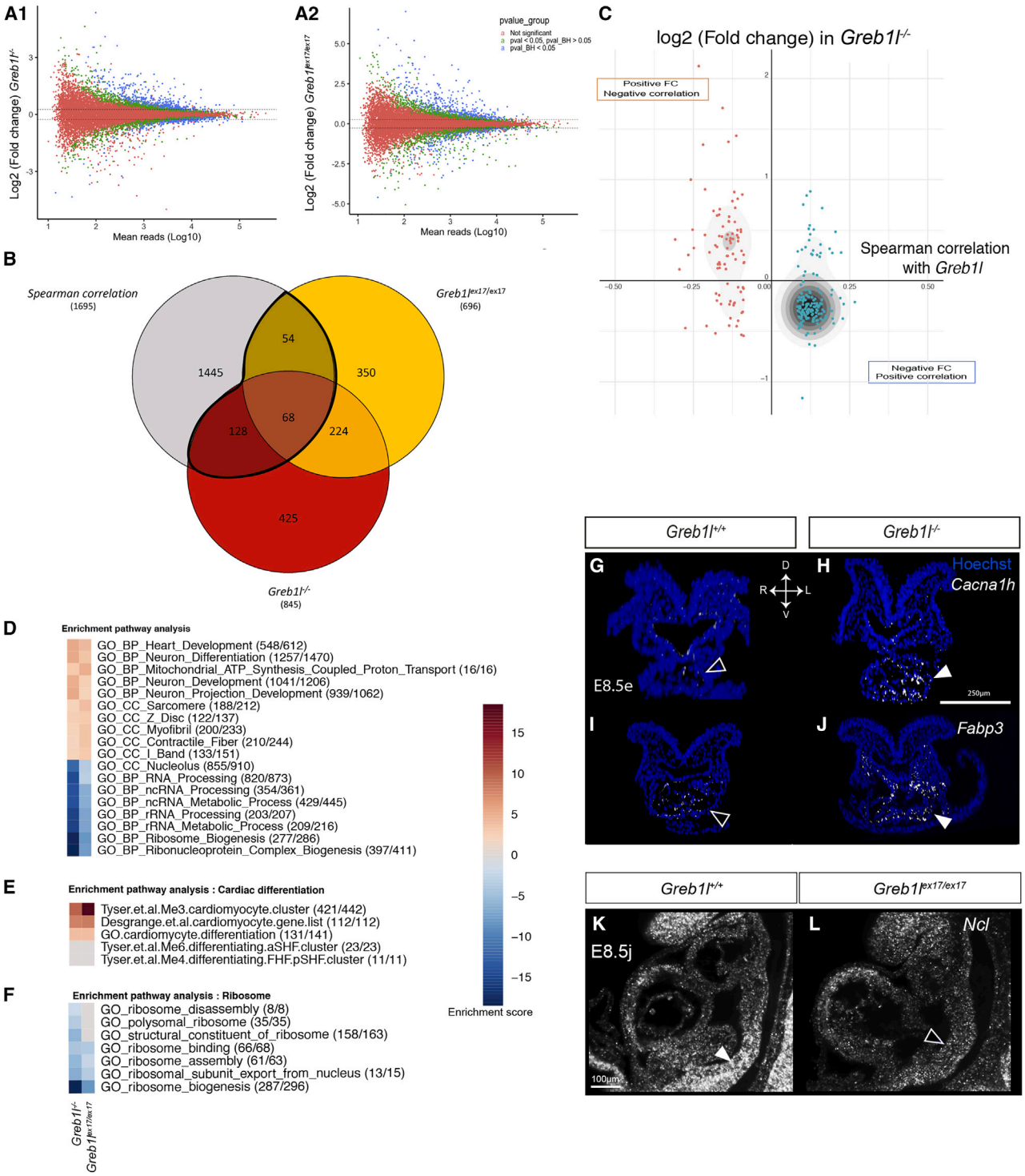

Figure 5. Transcriptomic changes in cardiomyocyte differentiation and ribosome biogenesis downstream of *Greb1l*

(A) MA plots representing relative gene expression between littermate controls and *Greb1l*$^{-/-}$ (A1) or *Greb1l*$^{ex17/ex17}$ (A2) mutants at E8.5e. Non-significant differential expression is represented in red, differential expression in green (p value < 0.05), and blue (Benjamini-Hochberg [BH]-corrected p value < 0.05, DEseq2, n = 4 controls each, 4 *Greb1l*$^{-/-}$ mutants, 4 *Greb1l*$^{ex17/ex17}$ mutants).

(B) Venn diagram comparing differentially expressed genes in *Greb1l*$^{ex17/ex17}$ (yellow) and *Greb1l*$^{-/-}$ (red) mutants with genes correlated with *Greb1l* levels in single wild-type embryonic cardiac cells (gray, see also Figure 2G). The 249 overlapping genes (excluding *Greb1l*) used for further analysis are outlined in bold.

poles (Figures 7E, 7F, and S4K), specifically in the inferior outflow tract and dorsal right atrium that are labeled by *RARE-lacZ* (Figures 7G and 7H). Thus, we detect defects in cardiomyocyte differentiation at the poles of the heart tube, where cells ingress to elongate the tube, likely leading to the growth arrest in the outflow tract at E10.5.

Taken together, our transcriptomic analyses and validations demonstrate a function of *Greb1l* in promoting ribosome biogenesis and controlling cell differentiation, to maintain the pool of precursor cells required for the elongation of the heart tube.

DISCUSSION

We have identified the role of *Greb1l* in maintaining a reservoir of precursor cells, which supplies the heart tube and shapes it. With quantitative spatiotemporal gene expression analyses, we show that *Greb1l* is expressed transiently in early cardiac precursors at E8.5c–f, overlapping with RA signaling. It promotes ribosome biogenesis and controls cell differentiation, overall maintaining the architecture and specification of cardiac precursor cells. The absence of *Greb1l* prevents the elongation of the outflow tract after E9.5 and reduces the distance between the tube poles. This is predictive of heart tube remodeling after heart looping, including torsion of the atrioventricular canal and supero-inferior ventricles. By characterizing a mouse model of crisscross heart, our work thus identifies the embryological mechanisms for this congenital heart defect.

Heart morphogenesis relies on the formation and shaping of an embryonic tube. The rightward looping of the tube is important for positioning the right ventricle and thus the overall alignment of cardiac chambers.[11,23,49] Our analysis of *Greb1l* mutants now indicates that the position of ventricles is not fixed after heart looping and that later growth of the heart tube can further modulate ventricle position. We thus uncover an aspect of heart morphogenesis, corresponding to the maintenance of chamber position subsequent to heart looping. Heart looping is determined by mechanical constraints during tube growth, such that tube deformation is primarily driven by a buckling mechanism.[11,49] Similarly, for the maintenance of chamber position, we find that growth of the heart tube, by ingression of precursor cells from the heart field, is essential. Impairment of growth in the absence of *Greb1l* generates abnormal mechanical constraints, which remodel the heart tube after heart looping. Another parameter of tube remodeling both during looping[11] and thereafter as shown here, is the distance between the poles. This is the main parameter associated with supero-inferior ventricles in *Rdh10* mutants. However, supero-inferior ventricles are fully penetrant, when both pole distance and outflow tract growth are affected in *Greb1l* mutants.

Abnormal ventricle position is classically associated with the heterotaxy syndrome,[9,50] which results from impaired left-right signaling.[51–53] However, crisscross heart is anatomically different from heterotaxy, as primarily defined by crossing of atrioventricular connections.[5,7] Our results highlight distinct morphogenetic and molecular mechanisms for ventricle malposition in crisscross heart, compared with heterotaxy. Whereas heterotaxy is associated with defective heart looping,[10,23,54–56] we show that crisscross heart is not. In addition, heterotaxy results from impaired left-right signaling upon mutations in ciliary genes or in Nodal pathway components,[51–53] whereas we identify a distinct gene network associated with crisscross heart, involving GREB1L.

Our quantification of shape changes in a unique mouse model uncovers the pathological mechanisms for crisscross heart. This congenital heart defect is primarily a shortage of correctly specified precursor cells, which will most strikingly arrest the growth of the outflow tract. This explains why crisscross heart is frequently associated with malposition of the great arteries, pulmonary stenosis and right ventricle hypoplasia.[6,7] Hypoplasia is thus not an indirect effect of heart rotation as hypothesized previously.[8] As a consequence of growth anomalies and reduction in pole distance, the embryonic heart tube is remodeled. This includes a torsion of the tube at the level of the atrioventricular canal, which accounts for twisted atrioventricular connections in crisscross heart.[8] Our observations at sequential stages of development indicate that the timing of twisting is before heart septation, between E9.5 and E10.5, which differs from predictions by anatomists.[4,5] Thus, our analyses of *Greb1l* mutants provide a comprehensive mechanistic insight into crisscross heart and associated cardiac defects. However, crisscross heart is not always associated with supero-inferior ventricles.[7] This may reflect different degree of tube torsion,[6] or raise the possibility that ventricle position may be corrected by further growth of the heart after E10.5.

Elongation of the heart tube depends on the progressive incorporation of precursor cells from the dorsal pericardial wall, pharyngeal mesoderm and juxta-cardiac field abutting the

(C) Corresponding representation of the 249 genes, according to their fold change (FC) in *Greb1l*$^{-/-}$ mutants and their Spearman correlation coefficient (red, r < 0; blue, r > 0, see Figure 2G). Point density is represented by a gray scale. Genes positively correlated with *Greb1l* in wild-type cells are significantly downregulated in mutants, and vice versa. (n = 249, p < 0.0001, chi^2 test.)

(D) Heatmap representing the most enriched GO pathways, ordered according to their enrichment score (blue, negative; gray, null; red, positive) in *Greb1l*$^{-/-}$ (left column) and *Greb1l*$^{ex17/ex17}$ (right column) mutants compared with littermate controls. Numbers in parentheses indicate the fraction of genes considered in specific GO terms.

(E and F) Heatmaps of gene set enrichment associated with cardiac differentiation (E) and ribosome (F), represented as in (D). See gene lists in Tyser et al. and Desgrange et al.[15,23]

(G–J) Expression of cardiomyocyte genes *Cacna1h* (G and H) and *Fabp3* (I and J) in controls (G, I, n = 3 each) and *Greb1l*$^{-/-}$ mutants (H, J, n = 3 each) detected by whole-mount RNAscope ISH at E8.5e and shown in transverse sections. Filled and empty arrowheads point to high and low expression in the heart, respectively.

(K and L) Expression of the ribosomal maturation gene *Ncl* detected by whole-mount RNAscope ISH in controls (K, n = 3) and *Greb1*$^{ex17/ex17}$ mutants (L, n = 3) at E8.5j shown in sagittal sections. Filled and empty arrowheads point to high and low expression in the heart field, respectively. aSHF, anterior second heart field; A, anterior; D, dorsal; FDR, false discovery rate; FHF, first heart field; HF, heart field; L, left; LV, left ventricle; NT, neural tube; R, right; RV, right ventricle; OFT, outflow tract; P, posterior; pSHF, posterior second heart field SHF; second heart field. V, ventral.

See also Table S1; Figures S2–S4.

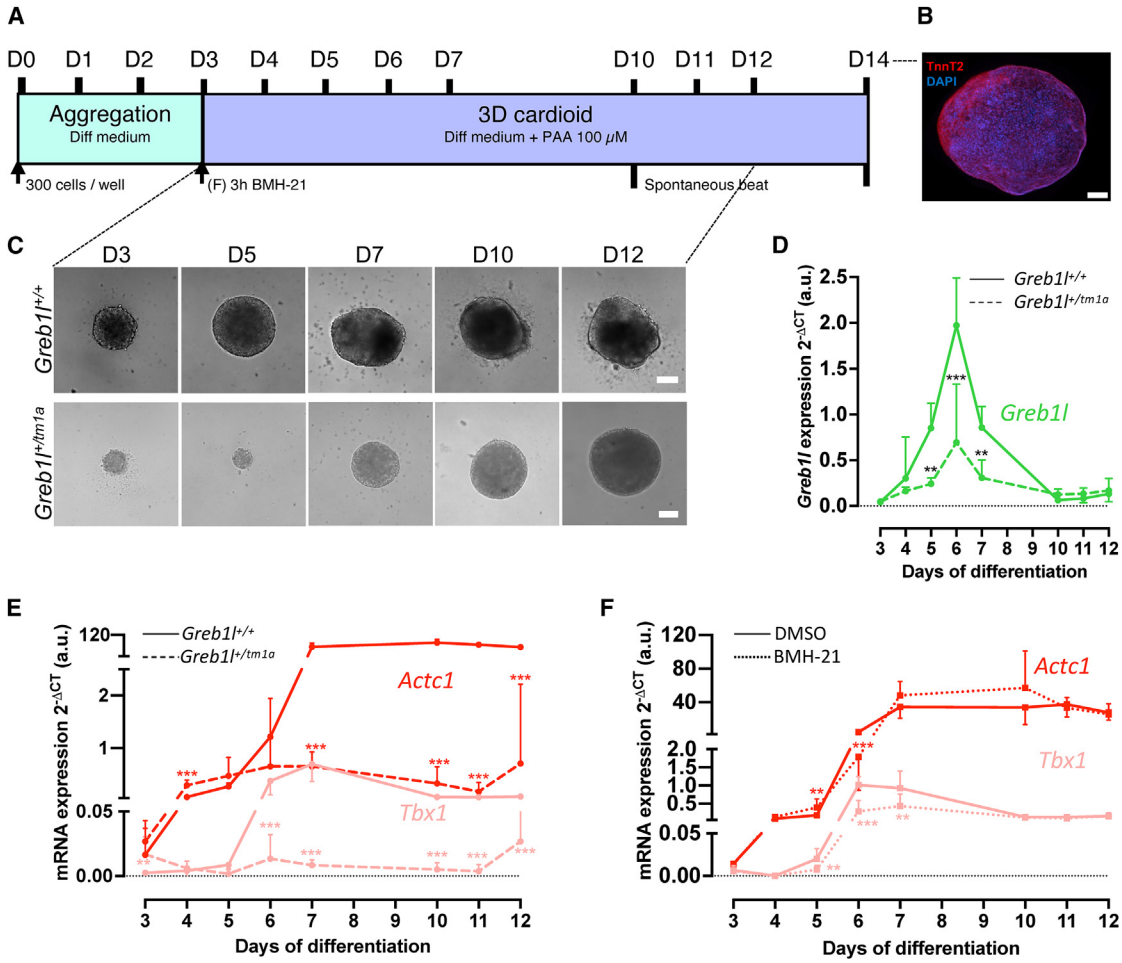

Figure 6. Defects in cardiac precursors and differentiation in a cardioid model with reduced *Greb1l* or ribosome biogenesis

(A) Timeline of the experimental design of cardioid production from mouse ES cells, and of their treatment.

(B) Immunostaining of cardioids at day 14, with the cardiomyocyte marker Tnnt2.

(C) Brightfield images of cardioids at the indicated timing, produced from control or *Greb1l*$^{+/tm1a}$ mutant ES cells.

(D and E) Corresponding quantification by RT-qPCR of the expression of *Greb1l* (D), the cardiomyocyte precursor gene *Tbx1* and the differentiated cardiomyocyte gene *Actc1* (E).

(F) Similar quantification of gene expression in wild-type cardioids treated with BMH-21, an inhibitor of ribosome biogenesis, or with the adjuvant (DMSO). $^{*}p < 0.05$, $^{**}p < 0.01$, $^{***}p < 0.001$ (8 replicates were analyzed, each as a pool of 8 cardioids, two-way ANOVA with random effects, tests comparing ΔCt mutants to controls are shown, n values are explained in the STAR Methods). Means and standard deviation are shown. Scale bars: 200 μm. D, day of culture; PAA, phospho-L-ascorbic acid; diff, differentiation.

See also Figure S5.

septum transversum.[14,15,57] Impairment of cardiomyocyte differentiation in *Nkx2-5*, *Tbx20*, *Mef2c*, or *Asb2* mutants, arrests heart development at E8.5–E9.5 and is embryonic lethal.[20,58–60] Decreased proliferation of heart precursors in *Fgf8* or *Hes1* mutants,[21,61] or disruption of the second heart field epithelial architecture in *Vangl2* and *Tbx1* mutants, which promotes ectopic cardiomyocyte differentiation,[12,13] shorten the outflow tract. These mutants, which survive to birth, manifest conotruncal malformations and ventricular septal defects. Anomalies in ventricle position seem to be visible at E9.5–E10.5 but have not been reported at birth, and neither crisscross heart. This indicates that impaired outflow tract growth not always results in abnormal remodeling of the cardiac tube. It remains to be investigated whether this is due to a threshold in the intensity of growth defects or in the specific timing of growth defects, since *Greb1l* is transiently expressed in heart precursors at E8.5c–f.

RA, which is known to regulate cardiomyocyte differentiation, heart field size,[26,42,62] and outflow tract growth,[26,35,36] had been previously identified in ES cells as an inducer of *Greb1l* expression, via a RARE sequence 13-kb upstream of the *Greb1l* promoter.[27] We now show *in vivo* that partial RA deficiency phenocopies *Greb1l* inactivation: *Rdh10* mutants have crisscross heart with supero-inferior ventricles and other models of transient RA deficiency, *CAGG-Cre-Esr1;RARa1*$^{-/-}$, *RXRa*$^{flox/flox}$ conditional mutants or RA-rescued *Aldh1a2* mutants, display outflow tract shortening.[35,36] However, *Greb1l* was not downregulated in *Aldh1a2* mutants, and targets of RA signaling were largely unchanged in *Greb1l* mutants. This suggests that GREB1L and

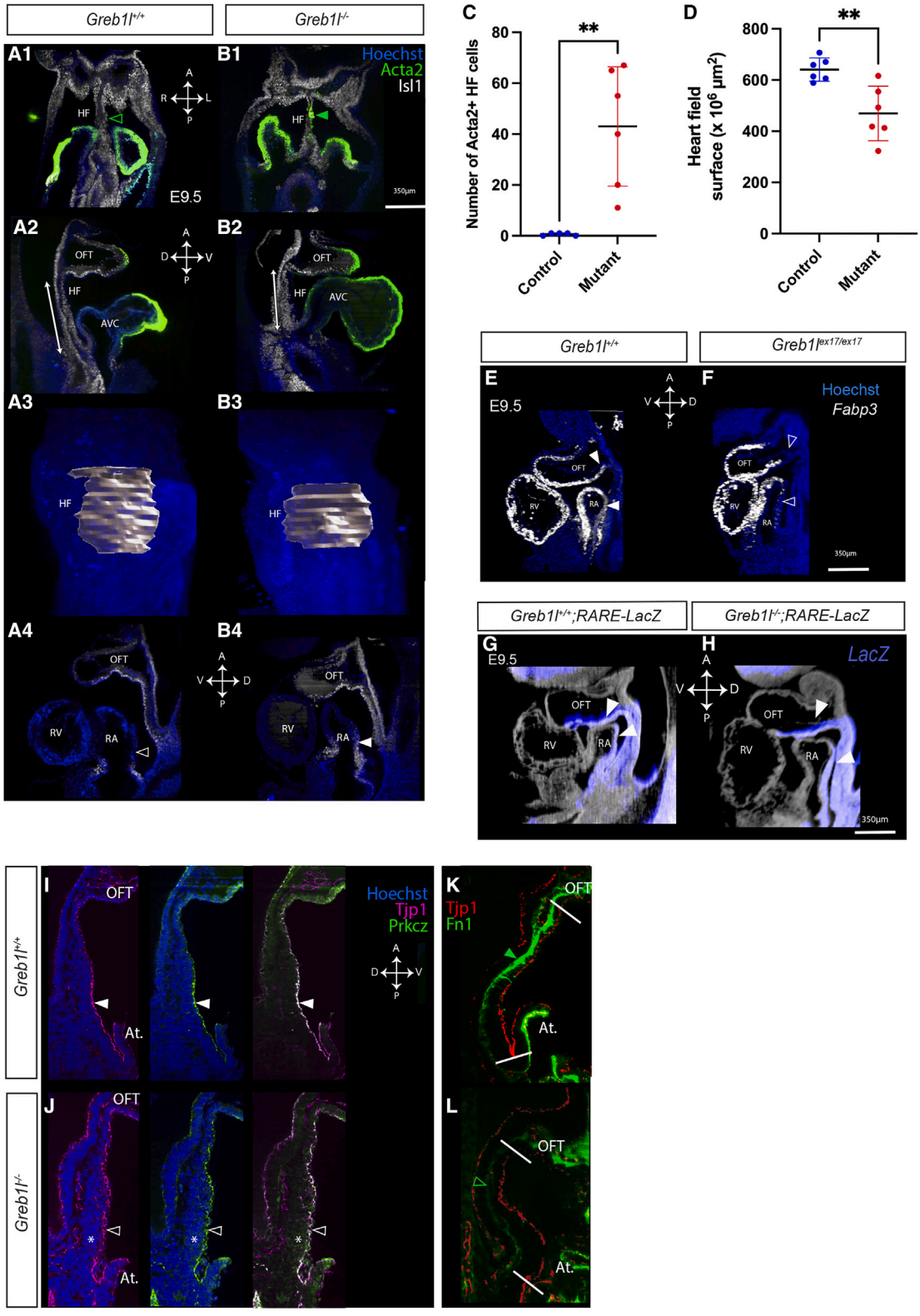
Greb1l+/+
Greb1l-/-
A1
B1
Hoechst
Acta2
Isl1
HF
E9.5
350µm
A2
B2
OFT
AVC
A3
B3
A4
B4
RV
RA
C
Number of Acta2+ HF cells
Control
Mutant
D
Heart field surface (x 10^6 µm^2)
Greb1l+/+
Greb1lex17/ex17
E
F
Fabp3
Greb1l+/+;RARE-LacZ
Greb1l-/-;RARE-LacZ
G
H
LacZ
I
J
K
L
Tjp1
Prkcz
Fn1
At.

RA signaling do not interact but are rather overlapping in regulating cardiac precursors with a similar spatiotemporal dynamics.

Our work on *Greb1l* in heart precursors reveals a novel dimension in the regulation of the reservoir of precursor cells. In addition to premature cardiomyocyte differentiation, transcriptomics of *Greb1l* mutants reveals reduced ribosome biogenesis. Although ribosomes are essential in every cell for protein synthesis, congenital ribosomopathies have tissue-specific phenotypes,[63,64] including conotruncal defects in Diamond Blackfan Anemia.[65] Ribosome levels have been shown to vary along cell trajectories, being lower in quiescent and differentiated cells but higher in intermediate cycling precursors,[66,67] and for example, higher in human ES cells compared with derived cardiomyocytes.[68] In agreement with these data, we show that impaired ribosome biogenesis in *Greb1l* mutants and cardiac organoids has secondary effects, with a longer term drop in cardiomyocyte differentiation and ultimately growth arrest of the outflow tract. The disorganization of the heart field further shows the incorrect specification of the reservoir of cardiac precursor cells in *Greb1l* mutants.

GREB1L has been previously associated with a broad spectrum of congenital defects in humans, such as urogenital defects, hearing impairment, and skeletal anomalies.[28] *Greb1l* mouse mutants are more severe and display general growth retardation, neural tube defects, and craniofacial anomalies[29] (Figure S1). All these phenotypes are also observed in ribosomopathies,[64] consistently with the role of *Greb1l* in regulating ribosome biogenesis. Despite the number of genetic variants in patient cohorts, *GREB1L* has remained a poorly characterized gene. Bioinformatics predictions (Uniprot, MobiDB[69]) indicate the presence of intrinsically disordered regions in GREB1L, compatible with a nucleolar localization,[70] where ribosomes are produced. Alternatively, by analogy with its paralogue GREB1, GREB1L could be involved in protein O-GlcNAcylation,[30] which is a modification required for the stability of ribonucleoproteins.[71] The processes regulated by *Greb1l* that we have discovered during cardiac development thus provide novel insight into a broad spectrum of congenital defects.

Limitations of the study

Our transcriptomic analyses and *in vivo* validation experiments highlight the role of *Greb1l* in ribosome biogenesis and cell differentiation. However, more knowledge of GREB1L protein and binding partners are required to determine whether this is a direct or indirect effect. We propose a mechanical remodeling of the heart tube following outflow tract growth arrest in mutants. This conclusion is based on correlations and awaits to be reinforced by targeted experiments or computer simulations. Our mouse model establishes *Greb1l* as a genetic determinant of crisscross heart. However, patients reported so far with *GREB1L* variants have no heart defect. Whether this reflects a milder pathogenicity compatible with life or differences between the human and mouse remains to be investigated. The human genetics of crisscross heart is pending and challenging, because of the difficulty to generate a large cohort of patients with a very rare defect.

STAR★METHODS

Detailed methods are provided in the online version of this paper and include the following:

- KEY RESOURCES TABLE
- RESOURCE AVAILABILITY
  - Lead contact
  - Materials availability
  - Data and code availability
- EXPERIMENTAL MODEL AND STUDY PARTICIPANT DETAILS
  - Animals
  - Cardioids
  - Patient recruitment and cardiac imaging
- METHOD DETAILS
  - β-galactosidase staining
  - RNA *in situ* hybridisation
  - Immunofluorescence
  - Proliferation and apoptosis assays
  - HREM (High-Resolution Episcopic Microscopy)
  - RNA isolation
  - RT-qPCR
  - RNA sequencing
  - Phenotyping of congenital heart defects
  - Tamoxifen injection
- QUANTIFICATION AND STATISTICAL ANALYSIS

Figure 7. Anomalies in the heart field and cardiomyocyte differentiation in *Greb1l* mutants at E9.5

(A and B) Expression of cardiomyocyte (Acta2) and heart field (Isl1) markers in controls (A) and *Greb1l*$^{-/-}$ mutants (B) detected by whole-mount immunofluorescence at E9.5, and shown in frontal (A1–B1, A3–B3) and sagittal (A2–B2, A4–B4) sections. Empty and filled arrowheads point to absent and ectopic cardiomyocyte differentiation in the heart field (green, A1–B1), or low and high Isl1 in the right atrium (white, A4–B4), respectively. 3D segmentation of the heart field is shown in (A3)–(B3).

(C) Corresponding quantification of Acta2-positive cells in the heart field. **$p < 0.01$ (n = 5 controls, 3 *Greb1l*$^{-/-}$ and 3 *Grebl1*$^{ex17/ex17}$ mutants, t test).

(D) Corresponding quantification of the heart field surface. **$p < 0.01$ (n = 6 controls, 3 *Greb1l*$^{-/-}$ and 3 *Grebl1*$^{ex17/ex17}$ mutants, t test). Means and standard deviations are shown.

(E and F) Expression of the cardiomyocyte gene *Fabp3* in controls (E, n = 5) and *Greb1l*$^{ex17/ex17}$ mutants (F, n = 5) detected by whole-mount RNAscope ISH at E9.5 and shown in sagittal sections. Filled and empty arrowheads point to high and low expression in the heart tube poles.

(G and H) HREM sagittal sections of *Greb1l*$^{+/+}$;*RARE-lacZ* controls and *Greb1l*$^{-/-}$;*RARE-lacZ* mutants at E9.5 stained for β-galactosidase activity (blue).

(I–L) Localization of apical (Tjp1 and Prkcz) and basal (Fn1) markers detected by whole-mount immunofluorescence in the E9.5 epithelial heart field of controls (n = 3) and *Greb1l*$^{-/-}$ mutants (n = 3). Filled and empty arrowheads point to regular and disorganized epithelial domains, respectively. The asterisk indicates abnormal cell alignment in mutants. Midline sagittal sections are shown, with the limits of the heart field outlined by a white line in (K) and (L). A, anterior; At, atrium; AVC, atrioventricular canal; D, dorsal; HF, heart field; L, left; LV, left ventricle; NT, neural tube; R, right; RA, right atrium; RV, right ventricle; OFT, outflow tract; P, posterior; V, ventral.

See also Figure S6.

- Quantification of RNAscope ISH signal
- Quantification of the geometry of the heart tube at E9.5 and E10.5
- Quantification of the immunolabelled heart field at E9.5
- Quantification of criss-cross and supero-inferior ventricles
- Computation of the torsion index
- Bioinformatics analyses of bulk RNA sequences
- Bioinformatics analyses of single cell RNA sequences
- Generalized Linear Model (GLM)
- Statistical analysis

SUPPLEMENTAL INFORMATION

Supplemental information can be found online at https://doi.org/10.1016/j.devcel.2023.09.006.

ACKNOWLEDGMENTS

We thank V. Benhamo, J. Terret, N. Agueeff, M. Cavaignac, M. Franco, and C. Cimper for generous technical assistance; T. Holm Bønnelykke for expert advice; A. Schedl, V. Ribes, E. Calo, and M. Cohen-Tannoudji for insightful discussions; A. Schedl, G. Comai, and V. Fraulob for the production of *Tg(RARE/Hspa1b-cre/ERT2)#Asc;R26*$^{mTmG/mTmG}$ and *Rdh10* mutant embryos; C. Jeanpierre and L. de Tomasi for Greb1l mutant mice; D. Conrozet and the histology platform of the SFR Necker; S. Dupichaud and the cell imaging platform; N. Goudin and the image analysis platform; C. Bole-Feysot and M. Zarhrate of the genomics platform; N. Cagnard and the bioinformatics platform; and Y. Zimmermann and the LEAT animal facility. This work was supported by core funding from the Institut Pasteur and INSERM, state fundings from the Agence Nationale de la Recherche under ''Investissements d'avenir'' program (ANR-10-IAHU-01, ANR-10-LABX-73-01 REVIVE), grants from the ANR (ANR-21-CE14-0062-01), and the Fondation Française de Cardiologie to S.M.M., the MSD-Avenir fund (Devo-Decode project), and the AXA Research Fund. S.B. has benefited from an MD-PhD fellowship of the Institut *Imagine*, supported by State funding from the ANR under ''Investissements d'avenir'' program (ANR-10-IAHU-01) and the Fondation Bettencourt-Schueller, and training from the Ecole Doctorale FIRE – Programme Bettencourt-Schueller. A.B., F.R., D.B., and L.H. are supported by the APHP. A.D. is an INSERM researcher, and S.M.M. is an INSERM research director.

AUTHOR CONTRIBUTIONS

Conceptualization, S.B. and S.M.M.; methodology, S.B., J.-F.L.G., E.P., S.S., and S.M.M.; software, J.-F.L.G. and E.P.; formal analysis, S.B., A.B., E.P., C.M., A.D., and L.H.; investigation, S.B., A.B., C.M., S.S., L.G., and A.D.; resources: W.K., L.H., F.R., S.Z., C.B., and D.B.; writing – original draft, S.M.M.; writing – review & editing, all authors; visualization, S.B., A.B., A.D., C.M., and E.P.; supervision, S.M.M. and S.B.; project administration, S.M.M.; funding acquisition, S.M.M., S.B., and A.B.

DECLARATION OF INTERESTS

The authors declare no competing interests. J.F.L.G. has additional corporate affiliations, as the director of LGC SA, Alma Group, and Faure Herman.

INCLUSION AND DIVERSITY

We support inclusive, diverse, and equitable conduct of research.

Received: February 2, 2022
Revised: April 28, 2023
Accepted: September 20, 2023
Published: October 17, 2023

REFERENCES

1. Desgrange, A., Le Garrec, J.F., and Meilhac, S.M. (2018). Left-right asymmetry in heart development and disease: forming the right loop. Development *145*, dev162776. https://doi.org/10.1242/dev.162776.
2. Houyel, L., and Meilhac, S.M. (2021). Heart development and congenital structural defects. Annu. Rev. Genomics Hum. Genet. *22*, 257–284.
3. Sanders, S. (2003). Crisscross Heart. Orphanet Encyclopedia.
4. Anderson, R.H., Shinebourne, E.A., and Gerlis, L.M. (1974). Crisscross atrioventricular relationships producing paradoxical atrioventricular concordance or discordance. Their significance to nomenclature of congenital heart disease. Circulation *50*, 176–180.
5. Anderson, R.H. (1982). Crisscross hearts revisited. Pediatr. Cardiol. *3*, 305–313. https://doi.org/10.1007/BF02427032.
6. Freedom, R.M., Culham, G., and Rowe, R.D. (1978). The crisscross and superoinferior ventricular heart: an angiocardiographic study. Am. J. Cardiol. *42*, 620–628. https://doi.org/10.1016/0002-9149(78)90632-X.
7. Manuel, D., Ghosh, G., Joseph, G., Lahiri, Aw., and George, P.V. (2018). Crisscross heart: transthoracic echocardiographic features. Indian Heart J. *70*, 71–74. https://doi.org/10.1016/j.ihj.2017.03.008.
8. Seo, J.W., Yoo, S.J., Ho, S.Y., Lee, H.J., and Anderson, R.H. (1992). Further morphological observations on hearts with twisted atrioventricular connections (crisscross hearts). Cardiovasc. Pathol. *1*, 211–217. https://doi.org/10.1016/1054-8807(92)90027-L.
9. Jacobs, J.P., Anderson, R.H., Weinberg, P.M., Walters, H.L., Tchervenkov, C.I., Del Duca, D., Franklin, R.C., Aiello, V.D., Béland, M.J., Colan, S.D., et al. (2007). The nomenclature, definition and classification of cardiac structures in the setting of heterotaxy. Cardiol. Young *17* (*Supplement 2*), 1–28. https://doi.org/10.1017/S1047951107001138.
10. Vanpraagh, R., Ongley, P.A., and Swan, H.J.C. (1964). Anatomic types of single or common ventricle in man: morphologic and geometric aspects of 60 necropsied cases. Am. J. Cardiol. *13*, 367–386. https://doi.org/10.1016/0002-9149(64)90453-9.
11. Le Garrec, J.-F., Domínguez, J.N., Desgrange, A., Ivanovitch, K.D., Raphaël, E., Bangham, J.A., Torres, M., Coen, E., Mohun, T.J., and Meilhac, S.M. (2017). A predictive model of asymmetric morphogenesis from 3D reconstructions of mouse heart looping dynamics. eLife *6*, e28951.
12. Francou, A., Saint-Michel, E., Mesbah, K., and Kelly, R.G. (2014). TBX1 regulates epithelial polarity and dynamic basal filopodia in the second heart field. Development *141*, 4320–4331. https://doi.org/10.1242/dev.115022.
13. Ramsbottom, S.A., Sharma, V., Rhee, H.J., Eley, L., Phillips, H.M., Rigby, H.F., Dean, C., Chaudhry, B., and Henderson, D.J. (2014). Vangl2-regulated polarisation of second heart field-derived cells is required for outflow tract lengthening during cardiac development. PLoS Genet. *10*, e1004871. https://doi.org/10.1371/journal.pgen.1004871.
14. Kelly, R.G., Brown, N.A., and Buckingham, M.E. (2001). The arterial pole of the mouse heart forms from FGF10-expressing cells in pharyngeal mesoderm. Dev. Cell *1*, 435–440. https://doi.org/10.1016/S1534-5807(01)00040-5.
15. Tyser, R.C.V., Ibarra-Soria, X., McDole, K., Arcot Jayaram, S., Godwin, J., van den Brand, T.A.H., Miranda, A.M.A., Scialdone, A., Keller, P.J., Marioni, J.C., et al. (2021). Characterization of a common progenitor pool of the epicardium and myocardium. Science *371*. https://doi.org/10.1126/science.abb2986.
16. Zhang, Q., Carlin, D., Zhu, F., Cattaneo, P., Ideker, T., Evans, S.M., Bloomekatz, J., and Chi, N.C. (2021). Unveiling complexity and multipotentiality of early heart fields. Circ. Res. *129*, 474–487. https://doi.org/10.1161/CIRCRESAHA.121.318943.
17. Meilhac, S.M., and Buckingham, M.E. (2018). The deployment of cell lineages that form the mammalian heart. Nat. Rev. Cardiol. *15*, 705–724. https://doi.org/10.1038/s41569-018-0086-9.

18. Bertrand, N., Roux, M., Ryckebüsch, L., Niederreither, K., Dollé, P., Moon, A., Capecchi, M., and Zaffran, S. (2011). Hox genes define distinct progenitor sub-domains within the second heart field. Dev. Biol. *353*, 266–274. https://doi.org/10.1016/j.ydbio.2011.02.029.

19. Lescroart, F., Mohun, T., Meilhac, S.M., Bennett, M., and Buckingham, M. (2012). Lineage tree for the venous pole of the heart: clonal analysis clarifies controversial genealogy based on genetic tracing. Circ. Res. *111*, 1313–1322. https://doi.org/10.1161/CIRCRESAHA.112.271064.

20. Lyons, I., Parsons, L.M., Hartley, L., Li, R., Andrews, J.E., Robb, L., and Harvey, R.P. (1995). Myogenic and morphogenetic defects in the heart tubes of murine embryos lacking the homeo box gene Nkx2-5. Genes Dev. *9*, 1654–1666. https://doi.org/10.1101/gad.9.13.1654.

21. Park, E.J., Ogden, L.A., Talbot, A., Evans, S., Cai, C.-L., Black, B.L., Frank, D.U., and Moon, A.M. (2006). Required, tissue-specific roles for Fgf8 in outflow tract formation and remodeling. Development *133*, 2419–2433. https://doi.org/10.1242/dev.02367.

22. Palmquist-Gomes, P., and Meilhac, S.M. (2022). Shaping the mouse heart tube from the second heart field epithelium. Curr. Opin. Genet. Dev. *73*, 101896. https://doi.org/10.1016/j.gde.2021.101896.

23. Desgrange, A., Le Garrec, J.-F., Bernheim, S., Bønnelykke, T.H., and Meilhac, S.M. (2020). Transient nodal signaling in left precursors coordinates opposed asymmetries shaping the heart loop. Dev. Cell *55*, 413–431.e6. https://doi.org/10.1016/j.devcel.2020.10.008.

24. Bernheim, S., and Meilhac, S.M. (2020). Mesoderm patterning by a dynamic gradient of retinoic acid signalling. Philos. Trans. R. Soc. Lond. B Biol. Sci. *375*, 20190556. https://doi.org/10.1098/rstb.2019.0556.

25. De Bono, C., Thellier, C., Bertrand, N., Sturny, R., Jullian, E., Cortes, C., Stefanovic, S., Zaffran, S., Théveniau-Ruissy, M., and Kelly, R.G. (2018). T-box genes and retinoic acid signaling regulate the segregation of arterial and venous pole progenitor cells in the murine second heart field. Hum. Mol. Genet. *27*, 3747–3760. https://doi.org/10.1093/hmg/ddy266.

26. Duong, T.B., Holowiecki, A., and Waxman, J.S. (2021). Retinoic acid signaling restricts the size of the first heart field within the anterior lateral plate mesoderm. Dev. Biol. *473*, 119–129. https://doi.org/10.1016/j.ydbio.2021.02.005.

27. Simandi, Z., Horvath, A., Wright, L.C., Cuaranta-Monroy, I., De Luca, I., Karolyi, K., Sauer, S., Deleuze, J.-F., Gudas, L.J., Cowley, S.M., et al. (2016). OCT4 acts as an integrator of pluripotency and signal-induced differentiation. Mol. Cell *63*, 647–661. https://doi.org/10.1016/j.molcel.2016.06.039.

28. Schrauwen, I., Liaqat, K., Schatteman, I., Bharadwaj, T., Nasir, A., Acharya, A., Ahmad, W., Van Camp, G., and Leal, S.M. (2020). Autosomal dominantly inherited GREB1L variants in individuals with profound sensorineural hearing impairment. Genes *11*, 687. https://doi.org/10.3390/genes11060687.

29. De Tomasi, L., David, P., Humbert, C., Silbermann, F., Arrondel, C., Tores, F., Fouquet, S., Desgrange, A., Niel, O., Bole-Feysot, C., et al. (2017). Mutations in GREB1L cause bilateral kidney agenesis in humans and mice. Am. J. Hum. Genet. *101*, 803–814. https://doi.org/10.1016/j.ajhg.2017.09.026.

30. Shin, E.M., Huynh, V.T., Neja, S.A., Liu, C.Y., Raju, A., Tan, K., Tan, N.S., Gunaratne, J., Bi, X., Iyer, L.M., et al. (2021). GREB1: an evolutionarily conserved protein with a glycosyltransferase domain links ERα glycosylation and stability to cancer. Sci. Adv. *7*, eabe2470. https://doi.org/10.1126/sciadv.abe2470.

31. Mohun, T.J., and Anderson, R.H. (2020). 3D anatomy of the developing heart: understanding ventricular septation. Cold Spring Harb. Perspect. Biol. *12*, a037465.

32. Lin, A.E., Krikov, S., Riehle-Colarusso, T., Frías, J.L., Belmont, J., Anderka, M., Geva, T., Getz, K.D., and Botto, L.D.; National Birth Defects Prevention Study (2014). Laterality defects in the national birth defects prevention study (1998–2007): birth prevalence and descriptive epidemiology. Am. J. Med. Genet. A *164A*, 2581–2591. https://doi.org/10.1002/ajmg.a.36695.

33. Kramer, T.C. (1942). The partitioning of the truncus and conus and the formation of the membranous portion of the interventricular septum in the human heart. Am. J. Anat. *71*, 343–370. https://doi.org/10.1002/aja.1000710303.

34. Bajolle, F., Zaffran, S., Kelly, R.G., Hadchouel, J., Bonnet, D., Brown, N.A., and Buckingham, M.E. (2006). Rotation of the myocardial wall of the outflow tract is implicated in the normal positioning of the great arteries. Circ. Res. *98*, 421–428.

35. El Robrini, N., Etchevers, H.C., Ryckebüsch, L., Faure, E., Eudes, N., Niederreither, K., Zaffran, S., and Bertrand, N. (2016). Cardiac outflow morphogenesis depends on effects of retinoic acid signaling on multiple cell lineages. Dev. Dyn. *245*, 388–401. https://doi.org/10.1002/dvdy.24357.

36. Li, P., Pashmforoush, M., and Sucov, H.M. (2010). Retinoic acid regulates differentiation of the secondary heart field and TGFbeta-mediated outflow tract septation. Dev. Cell *18*, 480–485. https://doi.org/10.1016/j.devcel.2009.12.019.

37. Rhinn, M., Schuhbaur, B., Niederreither, K., and Dollé, P. (2011). Involvement of retinol dehydrogenase 10 in embryonic patterning and rescue of its loss of function by maternal retinaldehyde treatment. Proc. Natl. Acad. Sci. USA *108*, 16687–16692. https://doi.org/10.1073/pnas.1103877108.

38. Sirbu, I.O., Gresh, L., Barra, J., and Duester, G. (2005). Shifting boundaries of retinoic acid activity control hindbrain segmental gene expression. Development *132*, 2611–2622. https://doi.org/10.1242/dev.01845.

39. Niederreither, K., Vermot, J., Schuhbaur, B., Chambon, P., and Dollé, P. (2000). Retinoic acid synthesis and hindbrain patterning in the mouse embryo. Development *127*, 75–85.

40. Cunningham, T.J., Zhao, X., Sandell, L.L., Evans, S.M., Trainor, P.A., and Duester, G. (2013). Antagonism between retinoic acid and fibroblast growth factor signaling during limb development. Cell Rep. *3*, 1503–1511. https://doi.org/10.1016/j.celrep.2013.03.036.

41. Niederreither, K., Vermot, J., Messaddeq, N., Schuhbaur, B., Chambon, P., and Dollé, P. (2001). Embryonic retinoic acid synthesis is essential for heart morphogenesis in the mouse. Development *128*, 1019–1031.

42. Ryckebusch, L., Wang, Z., Bertrand, N., Lin, S.C., Chi, X., Schwartz, R., Zaffran, S., and Niederreither, K. (2008). Retinoic acid deficiency alters second heart field formation. Proc. Natl. Acad. Sci. USA *105*, 2913–2918. https://doi.org/10.1073/pnas.0712344105.

43. Sirbu, I.O., Zhao, X., and Duester, G. (2008). Retinoic acid controls heart anteroposterior patterning by down-regulating Isl1 through the Fgf8 pathway. Dev. Dyn. *237*, 1627–1635. https://doi.org/10.1002/dvdy.21570.

44. Cunningham, T.J., Chatzi, C., Sandell, L.L., Trainor, P.A., and Duester, G. (2011). Rdh10 mutants deficient in limb field retinoic acid signaling exhibit normal limb patterning but display interdigital webbing. Dev. Dyn. *240*, 1142–1150. https://doi.org/10.1002/dvdy.22583.

45. Niederreither, K., Subbarayan, V., Dollé, P., and Chambon, P. (1999). Embryonic retinoic acid synthesis is essential for early mouse post-implantation development. Nat. Genet. *21*, 444–448.

46. Berenguer, M., Meyer, K.F., Yin, J., and Duester, G. (2020). Discovery of genes required for body axis and limb formation by global identification of retinoic acid–regulated epigenetic marks. PLOS Biol. *18*, e3000719. https://doi.org/10.1371/journal.pbio.3000719.

47. D'Aniello, E., Rydeen, A.B., Anderson, J.L., Mandal, A., and Waxman, J.S. (2013). Depletion of retinoic acid receptors initiates a novel positive feedback mechanism that promotes teratogenic increases in retinoic acid. PLOS Genet. *9*, e1003689. https://doi.org/10.1371/journal.pgen.1003689.

48. Ginisty, H., Amalric, F., and Bouvet, P. (1998). Nucleolin functions in the first step of ribosomal RNA processing. EMBO J. *17*, 1476–1486. https://doi.org/10.1093/emboj/17.5.1476.

49. Patten, B.M. (1922). The formation of the cardiac loop in the chick. Am. J. Anat. *30*, 373–397. https://doi.org/10.1002/aja.1000300304.

50. Van Praagh, R. (1972). The segmental approach in diagnosis of congenital heart disease. Birth Defects (Orig. Artic. S.) *8*, 4.

51. Hummel, K.P., and Chapman, D.B. (1959). Visceral inversion and associated anomalies in the mouse. J. Hered. *50*, 9–13. https://doi.org/10.1093/oxfordjournals.jhered.a106870.

52. Meno, C., Shimono, A., Saijoh, Y., Yashiro, K., Mochida, K., Ohishi, S., Noji, S., Kondoh, H., and Hamada, H. (1998). lefty-1 is required for left-right determination as a regulator of lefty-2 and nodal. Cell *94*, 287–297. https://doi.org/10.1016/S0092-8674(00)81472-5.

53. Supp, D.M., Witte, D.P., Potter, S.S., and Brueckner, M. (1997). Mutation of an axonemal dynein affects left-right asymmetry in inversus viscerum mice. Nature *389*, 963–966. https://doi.org/10.1038/40140.

54. Campione, M., Steinbeisser, H., Schweickert, A., Deissler, K., van Bebber, F., Lowe, L.A., Nowotschin, S., Viebahn, C., Haffter, P., Kuehn, M.R., et al. (1999). The homeobox gene Pitx2: mediator of asymmetric left-right signaling in vertebrate heart and gut looping. Development *126*, 1225–1234.

55. De La Cruz, M.V., Anselmi, G., Cisneros, F., Reinhold, M., Portillo, B., and Espino-Vela, J. (1959). An embryologic explanation for the corrected transposition of the great vessels: additional description of the main anatomic features of this malformation and its varieties. Am. Heart J. *57*, 104–117. https://doi.org/10.1016/0002-8703(59)90360-6.

56. Yan, Y.-T., Gritsman, K., Ding, J., Burdine, R.D., Corrales, J.D., Price, S.M., Talbot, W.S., Schier, A.F., and Shen, M.M. (1999). Conserved requirement for EGF-CFC genes in vertebrate left-right axis formation. Genes Dev. *13*, 2527–2537. https://doi.org/10.1101/gad.13.19.2527.

57. Domínguez, J.N., Meilhac, S.M., Bland, Y.S., Buckingham, M.E., and Brown, N.A. (2012). Asymmetric fate of the posterior part of the second heart field results in unexpected left/right contributions to both poles of the HeartNovelty. Circ. Res. *111*, 1323–1335. https://doi.org/10.1161/CIRCRESAHA.112.271247.

58. Lin, Q., Schwarz, J., Bucana, C., and Olson, E.N. (1997). Control of mouse cardiac morphogenesis and myogenesis by transcription factor MEF2C. Science *276*, 1404–1407. https://doi.org/10.1126/science.276.5317.1404.

59. Métais, A., Lamsoul, I., Melet, A., Uttenweiler-Joseph, S., Poincloux, R., Stefanovic, S., Valière, A., Gonzalez de Peredo, A., Stella, A., Burlet-Schiltz, O., et al. (2018). Asb2α-Filamin A axis is essential for actin cytoskeleton remodeling during heart development. Circ. Res. *122*, e34–e48. https://doi.org/10.1161/CIRCRESAHA.117.312015.

60. Stennard, F.A., Costa, M.W., Lai, D., Biben, C., Furtado, M.B., Solloway, M.J., McCulley, D.J., Leimena, C., Preis, J.I., Dunwoodie, S.L., et al. (2005). Murine T-box transcription factor Tbx20 acts as a repressor during heart development, and is essential for adult heart integrity, function and adaptation. Development *132*, 2451–2462. https://doi.org/10.1242/dev.01799.

61. Rochais, F., Dandonneau, M., Mesbah, K., Jarry, T., Mattei, M.-G., and Kelly, R.G. (2009). Hes1 is expressed in the second heart field and is required for outflow tract development. PLoS One *4*, e6267. https://doi.org/10.1371/journal.pone.0006267.

62. Keegan, B.R., Feldman, J.L., Begemann, G., Ingham, P.W., and Yelon, D. (2005). Retinoic acid signaling restricts the cardiac progenitor pool. Science *307*, 247–249. https://doi.org/10.1126/science.1101573.

63. Luzzatto, L., and Karadimitris, A. (1998). Dyskeratosis and ribosomal rebellion. Nat. Genet. *19*, 6–7. https://doi.org/10.1038/ng0598-6.

64. Orgebin, E., Lamoureux, F., Isidor, B., Charrier, C., Ory, B., Lézot, F., and Baud'huin, M. (2020). Ribosomopathies: new therapeutic perspectives. Cells *9*, E2080. https://doi.org/10.3390/cells9092080.

65. Vlachos, A., Osorio, D.S., Atsidaftos, E., Kang, J., Lababidi, M.L., Seiden, H.S., Gruber, D., Glader, B.E., Onel, K., Farrar, J.E., et al. (2018). Increased prevalence of congenital heart disease in children with Diamond Blackfan anemia suggests unrecognized Diamond Blackfan anemia as a cause of congenital heart disease in the general population: A report of the Diamond Blackfan anemia registry. Circ. Genom. Precis. Med. *11*, e002044. https://doi.org/10.1161/CIRCGENETICS.117.002044.

66. Chau, K.F., Shannon, M.L., Fame, R.M., Fonseca, E., Mullan, H., Johnson, M.B., Sendamarai, A.K., Springel, M.W., Laurent, B., and Lehtinen, M.K. (2018). Downregulation of ribosome biogenesis during early forebrain development. eLife *7*, e36998. https://doi.org/10.7554/eLife.36998.

67. van Velthoven, C.T.J., and Rando, T.A. (2019). Stem cell quiescence: dynamism, restraint, and cellular idling. Cell Stem Cell *24*, 213–225. https://doi.org/10.1016/j.stem.2019.01.001.

68. Pereira, I.T., Spangenberg, L., Robert, A.W., Amorín, R., Stimamiglio, M.A., Naya, H., and Dallagiovanna, B. (2019). Cardiomyogenic differentiation is fine-tuned by differential mRNA association with polysomes. BMC Genomics *20*, 219. https://doi.org/10.1186/s12864-019-5550-3.

69. Necci, M., Piovesan, D., Dosztányi, Z., and Tosatto, S.C.E. (2017). MobiDB-lite: fast and highly specific consensus prediction of intrinsic disorder in proteins. Bioinformatics *33*, 1402–1404. https://doi.org/10.1093/bioinformatics/btx015.

70. Guillen-Chable, F., Bayona, A., Rodríguez-Zapata, L.C., and Castano, E. (2021). Phase separation of intrinsically disordered nucleolar proteins relate to localization and function. Int. J. Mol. Sci. *22*, 13095. https://doi.org/10.3390/ijms222313095.

71. Qin, W., Lv, P., Fan, X., Quan, B., Zhu, Y., Qin, K., Chen, Y., Wang, C., and Chen, X. (2017). Quantitative time-resolved chemoproteomics reveals that stable O-GlcNAc regulates box C/D snoRNP biogenesis. Proc. Natl. Acad. Sci. USA *114*, E6749–E6758. https://doi.org/10.1073/pnas.1702688114.

72. Rossant, J., Zirngibl, R., Cado, D., Shago, M., and Giguère, V. (1991). Expression of a retinoic acid response element-hsplacZ transgene defines specific domains of transcriptional activity during mouse embryogenesis. Genes Dev. *5*, 1333–1344. https://doi.org/10.1101/gad.5.8.1333.

73. Da Silva, F., Jian Motamedi, F., Weerasinghe Arachchige, L.C., Tison, A., Bradford, S.T., Lefebvre, J., Dolle, P., Ghyselinck, N.B., Wagner, K.D., and Schedl, A. (2021). Retinoic acid signaling is directly activated in cardiomyocytes and protects mouse hearts from apoptosis after myocardial infarction. eLife *10*, e68280. https://doi.org/10.7554/eLife.68280.

74. Muzumdar, M.D., Tasic, B., Miyamichi, K., Li, L., and Luo, L. (2007). A global double-fluorescent Cre reporter mouse. Genesis *45*, 593–605. https://doi.org/10.1002/dvg.20335.

75. Cao, N., Liu, Z., Chen, Z., Wang, J., Chen, T., Zhao, X., Ma, Y., Qin, L., Kang, J., Wei, B., et al. (2012). Ascorbic acid enhances the cardiac differentiation of induced pluripotent stem cells through promoting the proliferation of cardiac progenitor cells. Cell Res. *22*, 219–236. https://doi.org/10.1038/cr.2011.195.

76. Habib Geryes, B., Calmon, R., Khraiche, D., Boddaert, N., Bonnet, D., and Raimondi, F. (2016). Radiation dose reduction in paediatric coronary computed tomography: assessment of effective dose and image quality. Eur. Radiol. *26*, 2030–2038. https://doi.org/10.1007/s00330-015-4032-5.

77. Renier, N., Wu, Z., Simon, D.J., Yang, J., Ariel, P., and Tessier-Lavigne, M. (2014). iDISCO: a simple, rapid method to immunolabel large tissue samples for volume imaging. Cell *159*, 896–910. https://doi.org/10.1016/j.cell.2014.10.010.

78. McFarlane, L., Truong, V., Palmer, J.S., and Wilhelm, D. (2013). Novel PCR assay for determining the genetic sex of mice. Sex. Dev. *7*, 207–211. https://doi.org/10.1159/000348677.

79. Love, M.I., Huber, W., and Anders, S. (2014). Moderated estimation of fold change and dispersion for RNA-seq data with DESeq2. Genome Biol. *15*, 550. https://doi.org/10.1186/s13059-014-0550-8.

80. Wu, D., and Smyth, G.K. (2012). Camera: a competitive gene set test accounting for inter-gene correlation. Nucleic Acids Res. *40*, e133. https://doi.org/10.1093/nar/gks461.

81. Liberzon, A., Birger, C., Thorvaldsdóttir, H., Ghandi, M., Mesirov, J.P., and Tamayo, P. (2015). The Molecular Signatures Database (MSigDB) hallmark gene set collection. Cell Syst. *1*, 417–425. https://doi.org/10.1016/j.cels.2015.12.004.

82. Supek, F., Bošnjak, M., Škunca, N., and Šmuc, T. (2011). REVIGO summarizes and visualizes long lists of gene ontology terms. PLoS One *6*, e21800. https://doi.org/10.1371/journal.pone.0021800.

83. de Soysa, T.Y., Ranade, S.S., Okawa, S., Ravichandran, S., Huang, Y., Salunga, H.T., Schricker, A., del Sol, A., Gifford, C.A., and Srivastava, D.

(2019). Single-cell analysis of cardiogenesis reveals basis for organ-level developmental defects. Nature *572*, 120–124. https://doi.org/10.1038/s41586-019-1414-x.

84. Lun, A.T.L., McCarthy, D.J., and Marioni, J.C. (2016). A step-by-step workflow for low-level analysis of single-cell RNA-seq data with Bioconductor. F1000Res *5*, 2122. https://doi.org/10.12688/f1000research.9501.2.

85. Benjamini, Y., and Hochberg, Y. (1995). Controlling the false discovery rate: A practical and powerful approach to multiple testing. J. R. Stat. Soc. B Methodol. *57*, 289–300.

86. Mulder, K., and Klugkist, I. (2017). Bayesian estimation and hypothesis tests for a circular Generalized Linear Model. J. Math. Psychol. *80*, 4–14. https://doi.org/10.1016/j.jmp.2017.07.001.

87. Akaike, H. (1973). Information theory and an extension of the maximum likelihood principle. In International Symposium on Information Theory, B.N. Petrov and F. Csaki, eds., pp. 267–281.

88. Schindelin, J., Arganda-Carreras, I., Frise, E., Kaynig, V., Longair, M., Pietzsch, T., Preibisch, S., Rueden, C., Saalfeld, S., Schmid, B., et al. (2012). Fiji: an open-source platform for biological-image analysis. Nat. Methods *9*, 676–682. https://doi.org/10.1038/nmeth.2019.

89. de Chaumont, F., Dallongeville, S., Chenouard, N., Hervé, N., Pop, S., Provoost, T., Meas-Yedid, V., Pankajakshan, P., Lecomte, T., Le Montagner, Y., et al. (2012). Icy: an open BioImage informatics platform for extended reproducible research. Nat. Methods *9*, 690–696. https://doi.org/10.1038/nmeth.2075.